Chapter 1

Raman Spectra of Soft Modes in Ferroelectric Crystals

Takeshi Shigenari

Additional information is available at the end of the chapter

http://dx.doi.org/10.5772/60613

Abstract

The interpretation of Raman spectra of soft modes in ferroelectric crystals is not easy because of its over-damped line shape and the complicated temperature dependence near the transition temperature. There exist not a few cases which are difficult to determine the transition type is either order-disorder or displacive type. The main purpose of this paper is to point out the characteristics of Raman spectra of polar modes and several cautions for the analysis of soft modes. We discuss on some general properties of the susceptibility functions and also show possible reasons of confusion which might lead to the incorrect conclusions in the specific cases of KH_2PO_4 (KDP), ferroelectric $SrTiO_3$ and proton–ordered Ice crystals.

Keywords: Soft mode, Raman spectroscopy, Phase transition, Polar mode

1. Introduction

Historically, phase transitions in ferroelectric crystals have been explained by the *order–disorder type* mechanism that is similar to magnetic crystals. In the1950s, however, the idea of soft mode for *displacive-type* structural phase transitions was proposed by Anderson and others [1]. Since the1960s, with the advent of laser technology, laser Raman spectroscopy became one of the most powerful experimental methods for the study of soft mode particularly in ferroelectric crystals, partly because soft modes below T_c are always Raman-active [2]. An excellent review of soft mode spectroscopy in the early stage was given by Scott [3]. A theoretical textbook, *Scattering of Light by Crystals*, by Hayes and Loudon was published in 1978 [4].

A displacive-type transition is induced by the softening (decreasing frequency) of a particular lattice vibrational mode (phonon) toward the transition temperature T_c and eventually the

freezing of the mode pattern changes the symmetry of the crystal. The interpretation of a soft mode, however, is not easy because its Raman spectrum is often observed without any definite peak and becomes a broad quasi-elastic peak near T_c. Therefore, interpretations of Raman spectra of polar modes, such as soft modes in ferroelectric crystals must be carefully done. Otherwise, incorrect conclusions might be obtained. In the following sections, several examples related to this problem are shown for the cases of KDP, ferroelectric $SrTiO_3$, and proton-ordered Ice crystals.

2. Characteristics of polar phonons

2.1. General properties of Polar phonons

If the displacement of a phonon Q produces an electric dipole moment $\vec{\mu} = e^* Q$ (e^*: effective charge), the mode is called a polar mode or polar phonon. A soft mode is not always a polar mode, for example, the soft mode in the $\alpha - \beta$ transition of quartz (SiO_2) is nonpolar. However, for ferroelectric transitions it is always a polar mode.

Due to its interaction with any kind of electric field, the mechanism of the scattering of light from polar modes is much more complicated than nonpolar modes [4]. The Raman spectrum of polar phonons has several characteristics as follows (Fig.1):

i. Frequency of a polar phonon Q depends on the direction of its propagation vector $\vec{K}_p$ due to the depolarization field $\vec{E}_d \propto -\vec{\mu}/\varepsilon$. If $\vec{K}_p$ is perpendicular to $\vec{\mu}$, it is a transverse optic phonon (TO) and if $\vec{K}_p$ is parallel to $\vec{\mu}$, it is a longitudinal optic phonon (LO). Generally speaking, the frequency of LO is higher than TO because of the depolarization field. If the polar nature of Q is strong (and much stronger than the anisotropy of the crystal), large LO/TO splitting is expected to take place (Fig.1).

ii. As shown in Fig. 1(b), TO interacts with infrared (IR) photon and propagates as the coupled mode "polaritons". In Raman spectra, polaritons can be observed only with a very small angle forward-scattering geometry [5].

iii. In the IR spectra, reflectivity between LO and TO frequency is high and almost flat, while in Raman spectra they are observed as separate peaks (Fig. 1(d, e)).

2.2. General properties of soft modes

i. Above T_c, the soft mode is the lowest frequency TO phonon. Below T_c, the soft mode becomes a totally symmetric mode (A_1). Therefore, it is Raman-active. In typical cases, its frequency follows the equation

$$\omega_{TO}^2(q=0) = a\left|T - T_c\right| \tag{1}$$

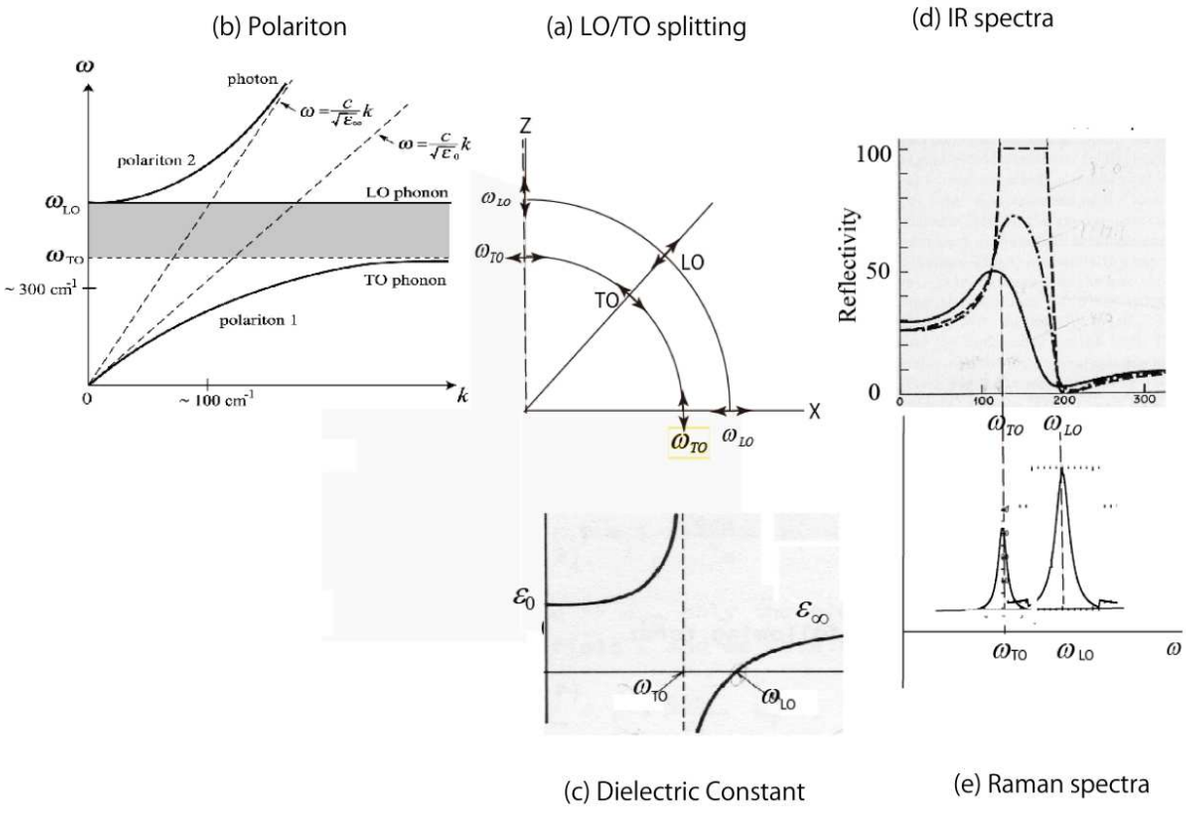

Figure 1. Various properties of polar LO and TO phonon in a cubic crystal. (a) LO/TO splitting in space, (b) dispersion of polariton, (c) dielectric constant, (d) IR reflection spectra, and (e) Raman spectrum.

ii. If the soft mode above T_c is degenerate, the degeneracy is lifted below T_c and one of them is totally symmetric (A_1) but A_1 is not necessarily the lowest frequency mode as in the $SrTiO_3$-18 case in section 5.2. Other split modes may or may not be Raman-active [6].

iii. Raman spectra of soft modes in the ferroelectric phase ($T < T_c$) depends on the angle between the spontaneous polarization $\vec{P}$ and the phonon propagation direction $\vec{K}_p$ because of the effect of the depolarization field $\vec{E}_d \propto -\vec{P}/\varepsilon$ as in the $SrTiO_3$ (section 5.2).

iv. Soft mode frequencies ω_{TO} and ω_{LO} are related to the dielectric constant via LST (Lyddayne–Sacks–Teller) relation.

$$\left(\omega_{TO}/\omega_{LO}\right)^2 = \varepsilon_\infty/\varepsilon_0 \tag{2}$$

iv. Integrated intensity of the soft mode Raman spectra is related to the *real part* of the low frequency dielectric constant $\varepsilon(\omega)$ via Kramers–Krong relation and Eq. (4) in the next section,

$$\mathrm{Re}\,\varepsilon(\omega)-\varepsilon_{\infty}=\frac{2}{\pi}P\int_{0}^{\infty}\frac{\omega'}{\omega'^{2}-\omega^{2}}\left(\frac{I(\omega')}{n(\omega')+1}\right)d\omega' \tag{3}$$

An example of this relation was demonstrated in the case of KDP [7].

3. Susceptibility $\chi_Q(\omega, T)$ for soft mode

3.1. Intensity and line shape of Raman spectra

Temperature and frequency dependence of Raman spectrum is represented by the imaginary part of the susceptibility $\chi_Q(\omega, T)$, which is the response of a phonon Q to its conjugate force f_Q.

$$I_S(\omega,T)\propto\left[n(\omega,T)+1\right]\mathrm{Im}\,\chi_Q(\omega,T) \tag{4}$$

or

$$\mathrm{Im}\chi_Q(\omega,T)=\frac{I_S(\omega,T)}{n(\omega,T)+1}=\frac{I_{AS}(\omega,T)}{n(\omega,T)} \tag{5}$$

where $I_S(\omega, T)$ and $I_{AS}(\omega, T)$ are intensity of Stokes and anti-Stokes side spectrum, respectively, and $n(\omega, T)=[\exp(\hbar\omega/k_BT)-1]^{-1}$ is the Bose factor. It should be noted that the approximations, $\hbar\omega/k_BT>>1$ or $\hbar\omega/k_BT<<1$, cannot be used for the soft mode.

In most cases, spectra are analyzed using either the so-called Damped Harmonic Oscillator (DHO) model for displacive-type transitions

$$\chi_Q(\omega)=\chi_Q(0)\frac{\omega_0^2}{\omega_0^2-\omega^2-i\omega\gamma} \tag{6}$$

or the Debye model (DB) for the relaxational behavior of order–disorder-type transitions,

$$\chi_Q(\omega)=\chi_Q(0)\frac{\gamma'}{\gamma'-i\omega} \tag{7}$$

where in ferroelectrics $\chi_Q(0)\approx C/(T-T_c)$ is proportional to the Curie constant C.

It seems rather strange, however, why these two formulas are exclusively used and what the meaning of the damping constant γ and γ' is. Since soft modes are often observed without any

apparent peaks, it is important to recognize the difference between the various forms of the susceptibilities. Thus, we discuss the more general formula of $\chi(\omega)$.

3.2. Generalized susceptibility and the stability limit

Phase transitions occur when the system becomes unstable. In other words, as $T \to T_c$, at least one of the poles of the $\chi(\omega)$ approaches the origin in the complex $\boldsymbol{\omega}$ plane. Typical traces are given in Fig. 2 for DHO, DB, and a more general case.

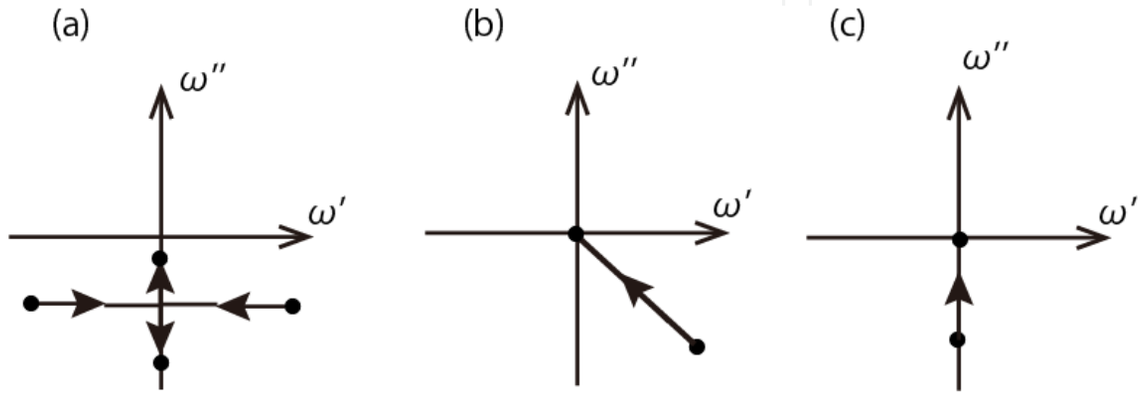

Figure 2. Motion of the pole of the susceptibility in the complex $\boldsymbol{\omega}$-plane as stability limit is approached. (a) Damped harmonic oscillator, (b) general case, (c) relaxation type (Debye).

As Van Vleck and Weisskopf showed in 1945 [8] for the case of microwave spectroscopy of gas, DHO and Debye types are qualitatively different in nature and DB cannot be obtained as a limit of vanishing characteristic frequency ω_0. It is because the γ' in DB (Eq. (7)) means the inverse relaxation time τ of the order parameter, which is a stochastic variable. In contrast, the γ in DHO (Eq. (6)) is a dynamical variable representing the damping proportional to the velocity of the order parameter. Nevertheless, in the field of Raman spectra, especially for an overdamped soft mode associated with structural phase transitions, it is often misleadingly stated that DHO smoothly reduced to DB by decreasing the ratio $\omega_0^2/\gamma \to 0$.

We note that the qualitative difference between DHO and DB originates from the fact that in DB the system is described for a finite time interval by neglecting the instantaneous change of the system. This "coarseness in the time domain" means that one cannot apply the Debye formula to the high frequency part of spectra. Therefore, the criteria, "high frequency tail of Raman spectra is proportional to ω^{-3} for DHO and ω^{-1} for DB" cannot be used to discriminate the displacive-type transitions from the order–disorder type.

Since a real system would not be represented by a single damping mechanism, we have proposed a more general form of susceptibility (GVWF) which includes two damping constants [9]. It is regarded as a generalization of the Van Vleck, Weisskopf, and Froehlich (VWF)-type susceptibility ($\gamma = \gamma'$).

$$\chi(\omega) = \chi(0)\frac{\omega_0^2 + \gamma\gamma' - i\gamma'\omega}{\omega_0^2 + \gamma\gamma' - i\left(\gamma + \gamma'\right)\omega - \omega^2} \tag{8}$$

In general, this form can be described by the two poles $\Omega_{1,2}$ in the complex $\boldsymbol{\omega}$ plane as follows:

$$\chi(\omega) = \frac{\chi(0)}{2}\left\{\frac{\Pi_1}{\Omega_1 - \omega} + \frac{\Pi_2}{\Omega_2 - \omega}\right\} \tag{9}$$

where

$$\Omega_{1,2} = -\frac{i\left(\gamma + \gamma'\right)}{2} \pm \sqrt{\omega_0^2 - \left(\gamma - \gamma'\right)^2/4}, \qquad \text{a}$$

$$\Pi_{1,2} = -i\gamma' \pm \left[\omega_0^2 + \gamma'(\gamma - \gamma')/2\right]\frac{1}{\sqrt{\omega_0^2 - \left(\gamma - \gamma'\right)^2/4}} \qquad \text{b} \tag{10}$$

The behavior of the poles in the complex $\boldsymbol{\omega}$ plane is shown in Fig. 3 for the case of the softening ($\omega_0 \to 0$) with constant γ and γ'.

a. If $\gamma >> \gamma' = 0$, GVWF corresponds to DHO and two poles move parallel to ω' axis and reach the imaginary axis when $\omega_0 = \gamma/2$ and they separately move on the ω'' axis, one toward the origin and another toward $-i\gamma$. In other words, if $\omega_0 < \gamma/2$, DHO cannot be discriminated from DB.

b. If $\gamma > \gamma' \neq 0$ (GVWF), two poles behave similar to the case (a) but even for $\omega_0 \to 0$ neither of them can reach the origin. They stop at $-i\gamma$ and $-i\gamma'$. The "intensity" of the two poles, $\Pi_{1,2}$, also changes; a mode toward $-i\gamma'$ increases, while the other pole gradually vanishes.

c. If $\gamma = \gamma'$ (VWF), two poles reach ω'' axis only when $\omega_0 = 0$.

d. If $\gamma < \gamma'$, behaviors of two poles are similar to the case (b) except that the "stronger" pole $-i\gamma'$ lies further from the origin than the weaker pole $-i\gamma$.

Behavior of various $\chi(\omega)$ can be understood in terms of the three parameters (ω_0, γ, γ') of GVWF. Figure 4 represents schematically the paths of the pole on approaching T_c. There are many paths leading to the divergence of $\chi(\omega)$. The stability limit leading to the phase transition takes place when one of the poles moves toward the origin of complex $\boldsymbol{\omega}$ plane (γ axis in Fig.4).

The pole of DHO moves in the DHO-plane (ω_0, γ, $\gamma' = 0$) as an ideal softening in displacive-type transitions. Ideal relaxation in order–disorder-type transitions (DB) corresponds to

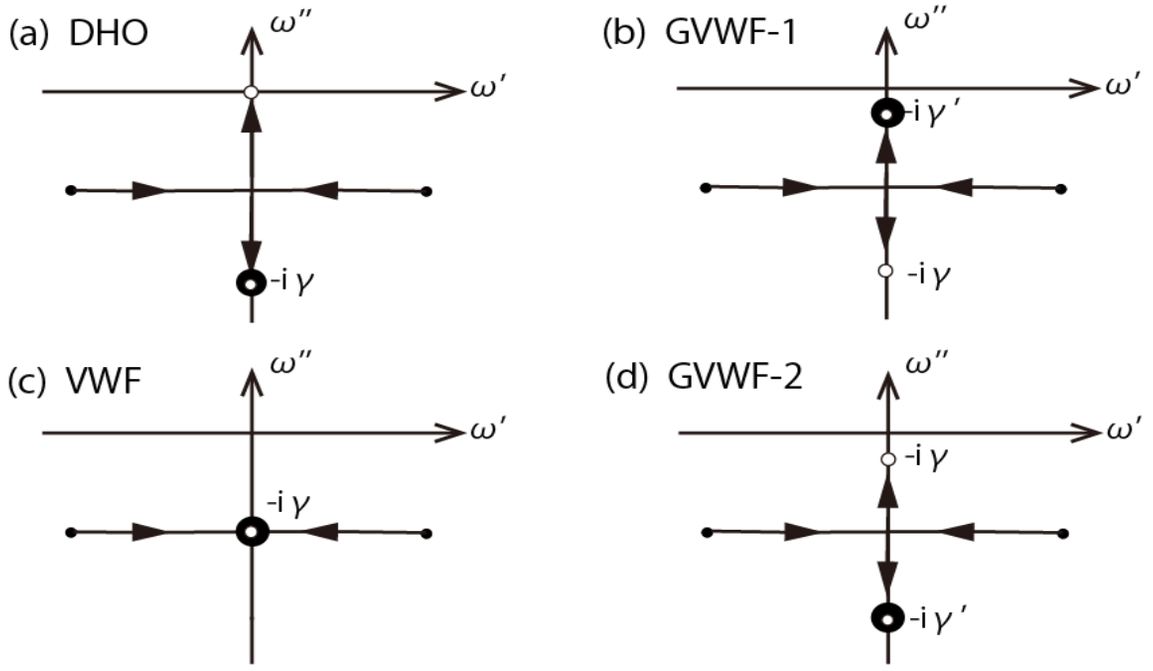

Figure 3. Behavior of the poles of the GVWF in the complex ω plane for $\omega_0 \to 0$ with fixed γ and γ'. (a) $\gamma >> \gamma'=0$, DHO; (b) $\gamma > \gamma' \neq 0$, GVWF; (c) $\gamma = \gamma'$, VWF; (d) $\gamma < \gamma'$, GVWF. Small white circles mean the position of the pole for $\omega_0=0$ and the big black circles denote the DB relaxation mode.

$\gamma' \to 0$ regardless of ω_0 and γ. The pole of VWF moves in the (ω_0, $\gamma=\gamma'$) plane. The hatched plane indicates the position where the pole reaches the imaginary axis. Thus, GVWF is the most general approach to the instability, indicating that the application of DHO or DB is not trivial but based on the hidden assumptions.

4. Phase transition of KDP (KH_2PO_4)

4.1. Raman spectrum of soft mode in KDP

The first experimental study of the soft mode was done by Kaminov and Damen in 1968 on the ferroelectric phase transition of KDP (KH_2PO_4) [10]. The structure changes from tetragonal D_{2d} ($I\bar{4}2d$) to orhorhombic C_{2v} ($Fdd2$). KDP is a unique ferroelectric crystal because of its large isotope effect on T_c, being 122K and 212K for KDP and DKDP (KD_2PO_4), respectively. Its origin was first attributed by Blinc et al. from the IR spectra to the tunneling of a proton between two PO_4 ions [11]. The soft mode has B_2 symmetry, which is Raman-active in the (xy) polarized spectrum. Contrary to most high-frequency modes, the lowest strong mode is a quasi-elastic mode that shows no peak down to zero frequency. Kaminov et al. analyzed the spectra by DHO and concluded that the characteristic frequency ω_0^2 goes to zero at T_c and suggested that the results are consistent with either the soft mode model [12] or the collective-tunneling-mode model [13, 14]. Their conclusions, however, were obtained simply assuming that the damping

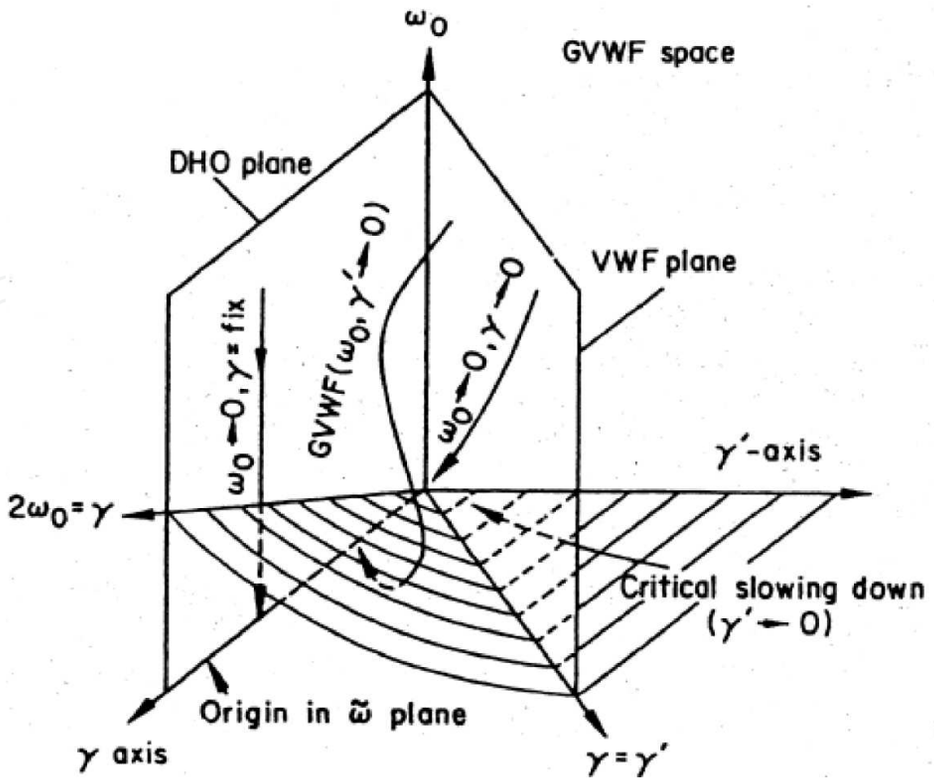

Figure 4. Behavior of the generalized susceptibility GVWF in $(\omega_0, \gamma, \gamma')$ space. Various paths of the pole to the origin of the complex ω plane are shown for DHO $(\omega_0 \to 0, \gamma = \text{const.})$, VWF $(\omega_0, \gamma = \gamma' \to 0)$, GVWF $(\omega_0, \gamma' \to 0)$, and DB $(\gamma' \to 0')$ cases.

constant γ is a constant. Quasi-elastic spectra are often observed in other crystals. (We shall call it simply as an overdamped mode unless it is necessary to discriminate them explicitly.) As mentioned in the previous section, it is not easy to analyze such a spectrum. It might be an overdamped soft mode (DHO) or a Debye-type relaxational mode (DB).

Temperature dependence of Raman spectra of overdamped soft modes is often shown in the *log scale* instead of the *linear scale* because of the significant increase of intensity as shown in Fig. 5(a) in linear scale. In the pioneering data by Kaminov et al. [10] and also in the papers by Tominaga et al. [16] for KDP and by Takesada et al. [17] for $SrTiO_3$ (see section 5), spectra are shown in log scale. We note, however, that this might mislead its interpretation. In the log scale spectra, the product of the Bose factor $n(\omega)$ and $\text{Im}\chi_Q$ is replaced by the sum of them. Then the low intensity part (i.e., the tail of the overdamped spectra) is apparently strengthened since the Bose factor is a monotonically increasing function toward infinity ($n(\omega=0)=\infty$), while $\text{Im}\,\chi_Q$ is zero at $\omega=0$ ($\text{Im}\chi_Q(\omega=0)=0$). As a consequence, the line shapes look quite different from that in the linear scale. For example, as in Fig. 5(b), the curvature of spectra changes from convex ($T<<T_c$) to concave ($T \approx T_c$). It looks as if there exist two components in the overdamped spectra. Figure 5(c) is the $\text{Im}\chi_Q(\omega, T)$ spectra corresponding to the linear scale spectra by removing the Bose factor contribution [15]. Its temperature dependence is very smooth toward

http://dx.doi.org/10.5772/60613

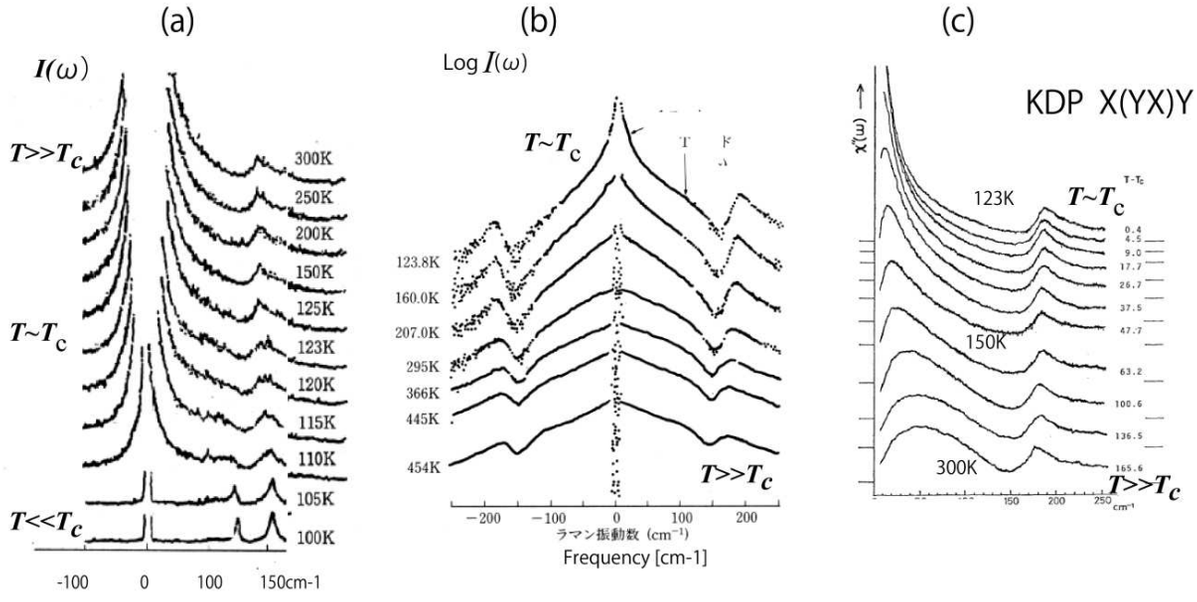

Figure 5. Temperature dependence of Raman spectra of KDP. (a) $I(\omega)$ in linear scale [15]. (b) Similar spectra $I(\omega)$ in log scale [16]. (c) Spectra of $\mathrm{Im}\ \chi_Q = I(\omega)/n + 1$ in linear scale. (See the text for the difference between these spectra.)

T_c without any qualitative change of the line shape. (The apparent peak in Fig. 5(c) is simply due to the fact $\mathrm{Im}\chi_Q(\omega=0)=0$.)

4.2. Displacive or order–disorder ?

Later studies by various groups however, revealed that the interpretation on the origin of the phase transition by Kaminov et al. [10] is not conclusive even from the Raman spectroscopic point of view. It still remains unclear whether it is a displacive type or an order–disorder type.

Difficulty of the interpretation of Raman spectra comes from the following reasons :

i. The low-frequency part of quasi-elastic spectra near T_c, can be fitted either by DHO as an overdamped soft mode or by DB as a relaxational mode. It can be fitted to any other function discussed in the previous section since from such a monotonic spectrum only a single parameter can be definitely determined, for example, ω_0^2/γ for the DHO model or γ for the DB model.

ii. Above T_c, because of the coupling with a higher-frequency mode at about 230 cm^{-1}, shown in Fig. 5, the line shape is distorted and cannot be well fitted to any single-mode line shape function. Interactions with modes near the quasi-elastic peak require the so-called coupled-mode analysis [18].

iii. Below T_c, another mode at about 100 cm^{-1} emerges from the overdamped mode observed by Kaminov et al., which suggests that the overdamped mode itself is not a single mode [19].

iv. Tominaga et al. insist that the phase transition of KDP is the order–disorder type [20]. The main evidence for their interpretation is based on the observation of extra Raman peaks above T_c in the 500–1000 cm^{-1} range, which should not be observed if the PO_4 units are the regular tetrahedra with S_4 symmetry. Thus, the existence of those peaks would indicate the PO_4 tetragonal unit is *not* regular but already distorted to C_2 symmetry above T_c. If it were true, the two different distortions of PO_4 (Fig. 6(b)) would cause the order–disorder transition. However, the observation of the extra peaks does not necessarily mean that PO_4 is statically distorted, because two protons vibrate coherently with PO_4 tetrahedron so that vibrational modes of the H_2-PO_4 system have C_2 symmetry and the extra peaks would be observed in Raman spectrum even if PO_4 is regular tetrahedra [21].

v. The role of protons in this transition is not clear in the order–disorder model. The coupled proton–PO_4 model proposed by Kobayashi [22] shown in Fig. 6(a) seems to be more realistic. As for the large difference of T_c between KDP and DKDP, no direct evidence for the proton tunneling as the origin of the isotope effect has so far been obtained. It was also revealed that there exists some difference of structure between KDP and DKDP. Details were discussed in [21]. Thus, it still remains unclear whether it is a displacive type or an order–disorder type.

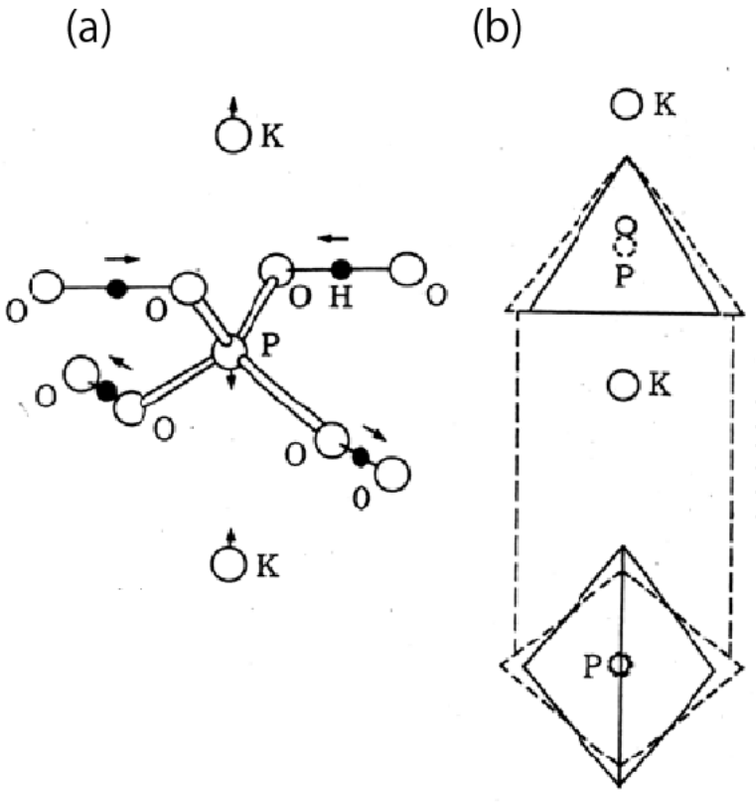

Figure 6. Two models for the ferroelectric transition in KDP. (a) Soft mode pattern of a proton–PO_4 coupled system proposed by Kobayashi [22]. (b) The order–disorder model of a deformed PO_4 [20].

4.3. Influence of the ferroelectric domain

Raman spectrum measures the macroscopic region of the sample. Therefore, in the Raman spectra of ferroelectric crystals the appearance of the domains with various scales and orientations in the sample should not be ignored. For example, a strange oscillatory behavior of the Raman intensity was observed in KDP. Raman intensity of A_1 mode, measured with the scattering geometry shown in Fig. 7(a), change oscillatory with temperature in the range $0<T_c-T<15K$ [23]. This behavior can be explained in terms of the interference of light reflected by the domain walls. Spontaneous polarizations $\pm\vec{P}$ in KDP are parallel to the c-axis and the thickness of 180 domain grows on cooling. The oscillatory behavior of Raman (Fig. 7(c)) is due to the periodical change of the polarization of light caused by the reflection from the domain walls and the birefringence between the neighbor domains as was confirmed by the similar oscillatory behavior the reflected light (Fig. 7(d)) [23].

The influences of domains in Raman spectra are also important in the case of more complicated domain structures in the case of STO18, discussed in section 5.2.

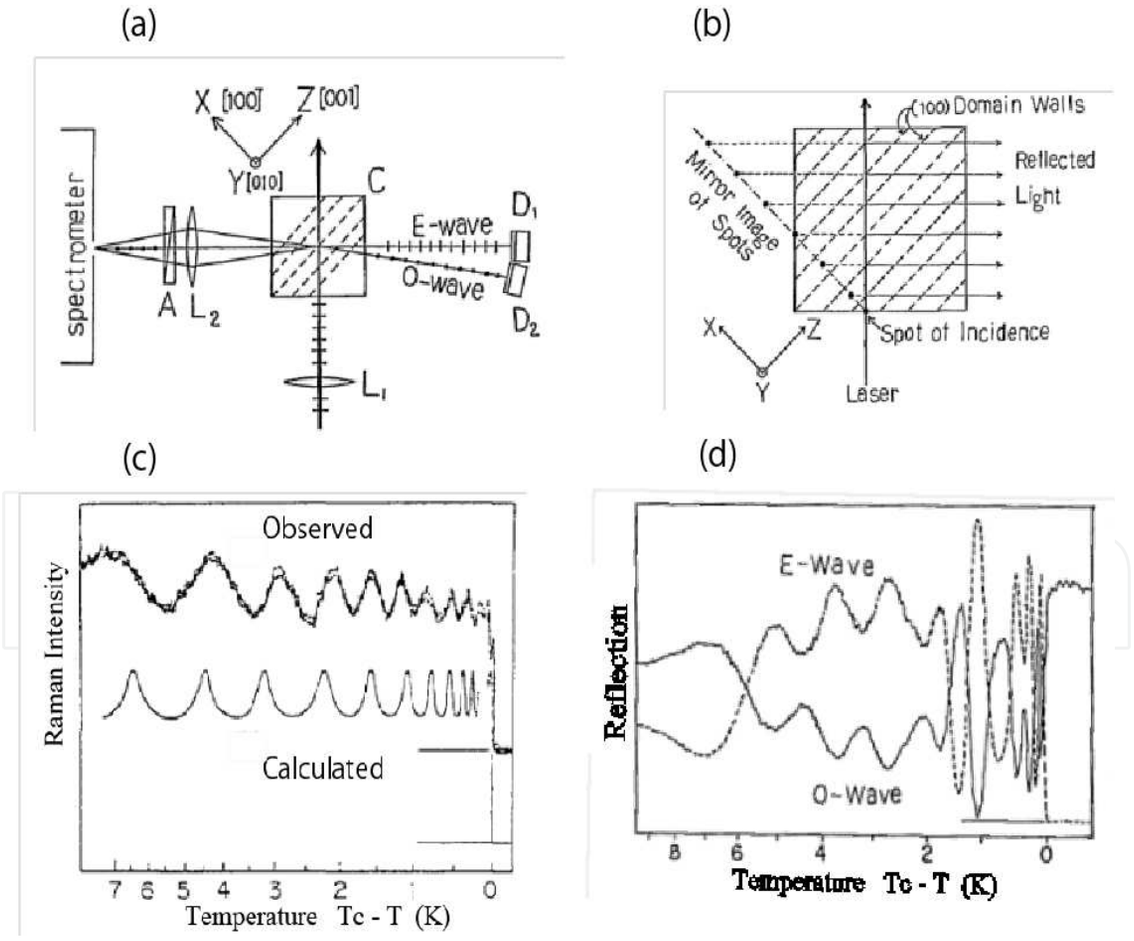

Figure 7. Influence of domains on Raman spectrum. (a) Scattering geometry. (b) Laser path and the reflection from domain walls. (c) Oscillatory change of Raman intensity with temperatture. (e) Intensity of the reflected light [23].

5. Ferroelectric $SrTiO_3$

$SrTiO_3$ is a typical crystal with perovskite structure (Fig. 8(a)) and it is easy to get a pure transparent single crystal. As a well-known incipient ferroelectric, it is one of the most widely studied dielectric crystals [24]. In 1999, Itoh et al. found the ferroelectricity in $SrTiO_3$ by the isotope substitution of O^{16} by O^{18} [25]. Since then, there has been considerable renewed interest in the low-temperature properties of $SrTiO_3$. Hereafter, we refer to $SrTiO_3^{16}$ and $SrTiO_3^{18}$ as STO16 and STO18, respectively. First, we will review the soft mode behavior in the normal STO16 and in the next subsection the soft mode in STO18 will be discussed.

5.1. Soft mode in STO16

$SrTiO_3$ undergoes a structural (anti-ferro-distortive) phase transition at T_0=105K from cubic $O_h^1(Pm\bar{3}m)$ to tetragonal $D_{4h}^{18}(4/mcm)$ structure. This transition is induced by the freezing of a zone boundary nonpolar soft mode $R_{25}^{'}$ (structural soft mode), which is an alternative rotational vibration of TO_6 octahedra around one of the cubic axes (Z-axis $[001]_c$) [26]. As shown in Fig. 8(b), the crystal axes in the tetragonal phase are rotated by 45° from the cubic axes and the unit cell is a rectangular parallelepiped elongated along one of the cubic Z-axes. It should be noted, therefore, that the multi-domain effect must be carefully taken into account since a sample below T_0 is usually consisted from a number of tetragonal domains with different Z-directions. It is especially important for the case of STO18 as we shall show in the next section. Below T_0 in the tetragonal phase, the triply degenerate structural soft mode splits into two Raman-active $A_{1g}+E_g$ modes and their frequencies increase on further cooling reaching 44 and 11 cm^{-1}, respectively.

Besides the "structural soft mode" there is another soft mode, the so-called ferroelectric soft mode in $SrTiO_3$. It is the lowest transverse mode (TO_1) among the 4 zone-center Γ_{15} modes in the cubic symmetry, which is known as the Slater mode (Fig. 8(a)). Frequency of the corresponding LO mode is much higher (170 cm^{-1}) than TO_1. The large LO/TO splitting indicates the very strong polar nature of this mode. Temperature dependence of the ferroelectric mode has been extensively studied. Above T_0 in the cubic phase, it is a doubly degenerate E_u mode regardless of the propagation directions $\vec{K}_p$. Below T_0 in the tetragonal phase, however, the symmetry of this mode depends on the $\vec{K}_p$. If it propagates along Z-axis, the degeneracy remains but when it propagates in the X-Y plane, TO_1 splits into $A_{2u}+E_u$ [27] (also see Fig. 12(a) in the next section).

The softening of A_{2u} and E_u was first observed by IR spectroscopy [28] and later confirmed by neutron scattering [29] and hyper-Raman scattering [27, 30]. Its frequency (90cm^{-1}) at room temperature decreases to about 15 cm^{-1} in low temperature. In spite of the significant softening, it rounds off at about 30 K and never freezes down to zero K. Thus, STO16 is known as quantum paraelectric crystal since quantum fluctuation at low temperatures hinders the freezing of the soft mode.

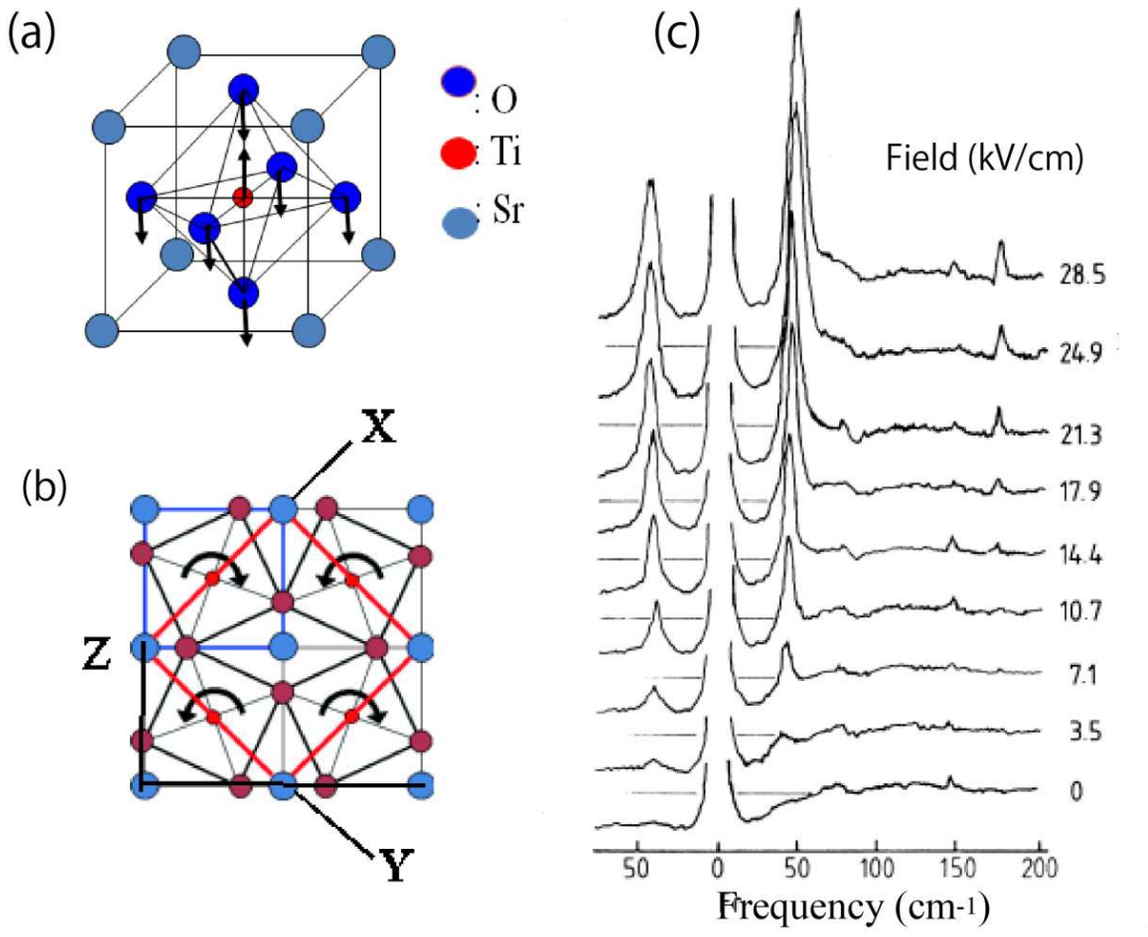

Figure 8. (a) Perovskite structure and the ferroelectric soft mode (Slater mode). (b) Blue and red squares are the unit cell in the cubic and the tetragonal phase, respectively. (c) Electric field effect on Raman spectra of ferroelectric soft mode in STO16 at T=101 K [32].

Although the ferroelectric soft mode is Raman-inactive, surprisingly it was found that if a DC electric field is applied its intensity and frequency drastically increase [31]. The field effect was observed even at higher temperature near T_0 as shown in Fig. 8(c) [32]. This is another evidence of the extremely strong polar nature of the ferroelectric soft mode in $SrTiO_3$. In other similar crystals, for example in $KNbO_3$, the effect is much weaker than in $SrTiO_3$ [33].

5.2. Soft mode in $SrTiO_3^{18}$ (STO18)

5.2.1. Propagation dependence of the soft mode in STO18

STO18 undergoes the structural phase transition from cubic to tetragonal at about T_0=108 K, which is slightly higher than T_0=105 K of STO16. On further cooling at T_c=24 K, however, STO18 transforms to the ferroelectric phase with orthorhombic structure (C_{2v}). [25] Ferroelectric properties of highly substituted STO18 (higher than 33%) were confirmed by the enormous increase of the dielectric constant and the appearance of the hysteresis curve.

All the samples used in many laboratories were provided from Itoh's laboratory. The samples are thin plates of size 0.3 x 2 (or 3) x 7 mm^3 with the widest plane $[110]_c$, and the longest and the shortest edges are parallel to $[001]_c$ and $[110]_c$, respectively. In the early stage, most samples used were not a single tetragonal domain but included many domains with different Z-directions. Thus, the reports measured with multi-domain samples were controversial and could not give consistent results.

Figure 9 is the summary of the temperature dependence of the soft mode frequency in STO18 measured by various experiments. The data are from samples with a single tetragonal domain except for the neutron diffraction.

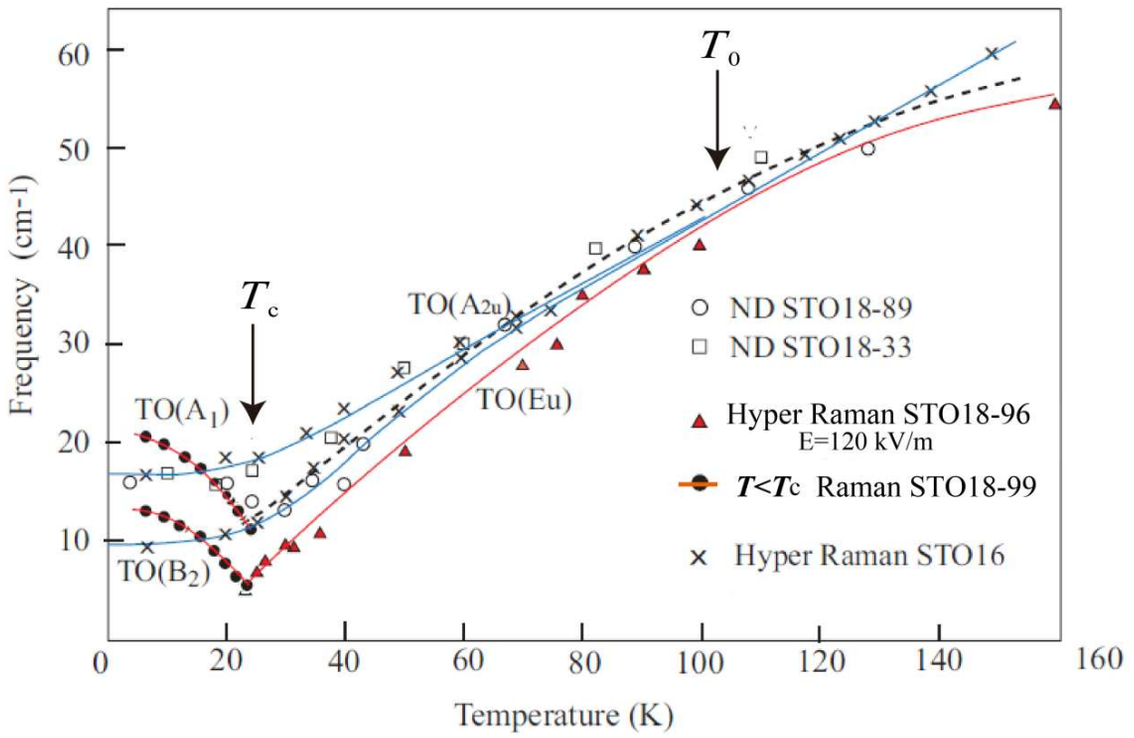

Figure 9. Temperature dependence of the ferroelectric soft mode of $SrTiO_3$. T_c of STO18 is slightly different for various experiments but here it is assumed to be about 24 K. The solid lines are guide for eyes. ○ and □ are neutron diffraction of STO18 [34]. × are hyper Raman of STO16 [35] and ▲ are hyper Raman of STO18 above T_c measured under the electric field [27]. ● are Raman scattering below T_c in STO18-99 [36]. Below T_c, only the Raman data clearly show the soft mode behavior in STO18.

Hyper Raman data under DC-electric field from STO18-96 show the softening similar to STO16 above T_c, but they do not give reliable data below T_c.[27] Neutron diffraction data hardly detect the influence of the phase transition [34]. Thus, the space group of STO18 below T_c has not yet been determined definitely. As we shall show later, it is probably because of the inhomogeneity of STO18 due to the existence of the paraelectric phase as a matrix of ferroelectric domains. Below T_c, only the Raman data succeeded in getting reliable soft mode frequencies [36]. Note that all these data show that the freezing of the soft mode (perfect softening) does *not* occur.

http://dx.doi.org/10.5772/60613

Later, highly substituted single-domain samples, STO18-99, became available. The results discussed below are the data obtained from such samples. For the correct assignment and interpretation, we found that the following features should be carefully taken into account [36]:

a. Temperature and polarization dependences of spectra are strongly dependent on the phonon propagation vector, $\vec{K}_p = \vec{K}_i - \vec{K}_s$ ($\vec{K}_i$ and $\vec{K}_s$ are the propagation vector of the incident and scattered photon, respectively).

b. Spectra measured in a single geometry or a single $\vec{K}_p$ is not enough for the correct assignment. Such a measurement would lead to incorrect conclusions.

c. The existence of the ferroelectric domains in the sample, particularly the direction of the spontaneous polarization $\vec{P}$ in the domains must be properly taken into account.

In the ferroelectric phase of STO18, five modes are observed in the low-frequency part below 50 cm^{-1} as one can see in Fig.10 and 11. Three of them are from the structural soft modes, as A_1 (from A_{1g}) at 44 cm^{-1} and A_2 and B_1 (from E_g) at 11 and 17.5 cm^{-1}, respectively. Since these modes are nonpolar, the line width is narrow and does not depend on $\vec{K}_p$ (Fig.11(b) and (c)). In contrast, the behavior of the ferroelectric soft modes, TO(A_1) and TO(B_2), very broad and sensitive to $\vec{K}_p$ (Fig.11). It is also sensitive to the scattering geometries. For example, the polarization dependence of the spectra with $\vec{K}_p$ // X at a temperature well below T_c (at about 7K) is shown for three different geometries in Fig.10. Note that in the geometry (c) of Fig.10, the VV(Z, Z) spectrum is quite different from other geometries, since even for the same $\vec{K}_p$, the selection rules are different for different geometries.

Spectra for $\vec{K}_p$ // Y (not shown in Fig.11) were found to be exactly the same as $\vec{K}_p$ // X, suggesting that there are two kinds of small domains with $\vec{P}$ // X and $\vec{P}$ // Y equally distributed in the sample, as we will discuss later.

In Fig. 11, the spectra for $\vec{K}_p$ // Z and $\vec{K}_p$ // X look similar except that there are two broad peaks in $\vec{K}_p$ // Z spectra while in $\vec{K}_p$ // X there is only one. Moreover, their temperature dependences are essentially different as we shall show in the next section.

It should be emphasized that the $\vec{K}_p$ // X + Y spectra (Fig.11(c)) are qualitatively different from other directions in the following two points: (1) The strong and broad peak at 20 cm^{-1} in the VV spectra of $\vec{K}_p$ // Z and $\vec{K}_p$ // X appears in $\vec{K}_p$ // X + Y at a lower frequency 17 cm^{-1}. This means that the depolarization field in $\vec{K}_p$ // X + Y is weaker than that in $\vec{K}_p$ // Z or $\vec{K}_p$ // X, so that the mode at 17 cm^{-1} is not a pure TO(A_1) mode. (2) In $\vec{K}_p$ // X + Y, there appear spurious modes (arrows in Fig. 11(c)) that are unable to assign to any mode in STO18. As we shall discuss later, these modes are originated from the matrix of the paraelectric phase.

Our final assignment of displacement and the symmetry of the ferroelectric soft modes are illustrated in Fig. 12(a) for temperature above T_c and in Fig. 12(b) for well below T_c. All the features of the observed spectra, including the subtle differences in the polarized spectra and the expected selection rules, were consistently explained *only* if the spontaneous polarization $\vec{P}$ is either parallel to the tetragonal axes X or Y. $\vec{P}$ cannot be along one of the cubic directions

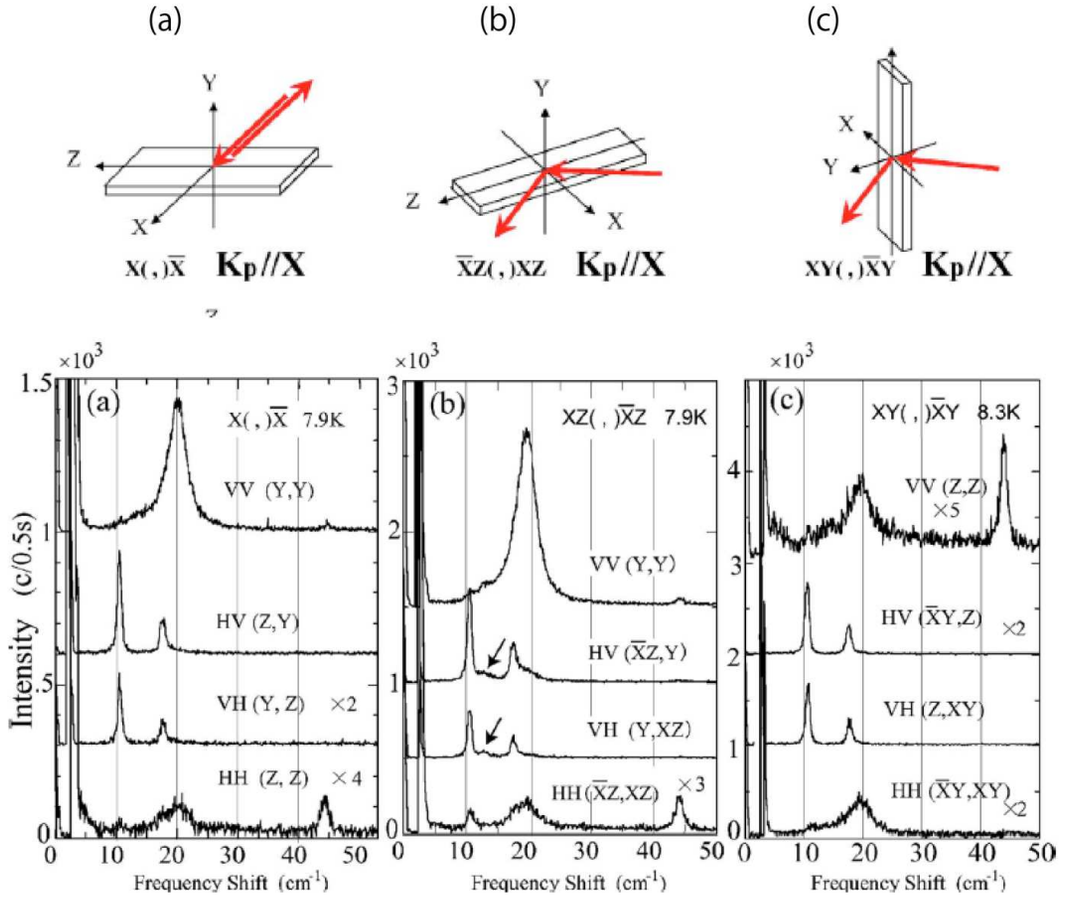

Figure 10. Three different scattering geometries for the same propagation direction, $\vec{K}_p$ // X. Broad mode at 20 cm^{-1} is $TO(A_1)$ and the shoulder in HV and VH of (b) (shown by arrows) is $TO(B_2)$ [36] In the geometry (c), the VV(Z, Z) spectrum is quite different from other geometries.

as one might expect for the Slater mode [26], since it is neither parallel to $X \pm Y$ (=[100]c or [010]c) nor Z (=$[001]_c$). If $\vec{P}$ were parallel to one of the cubic axes, observed spectra never satisfy any selection rules. Reason for this unexpected result will be given later.

As one can see in Fig. 12(b), the doubly degenerate TO(Eu) splits into $TO(A_1)$ + $TO(B_2)$ when it propagates along Z, but when it propagates in the X-Y plane, $TO(A_1)$ changes to $TO(B_1)$, of which displacement is perpendicular to $\vec{P}$. Since the displacement of $TO(A_1)$ is parallel to $\vec{P}$, it is reasonable that the frequency of $TO(A_1)$ (20 cm^{-1}) is higher than $TO(B_1)$ (17.5 cm^{-1}) and its intensity is stronger. Similar to the very strong external DC-field effect observed in STO16 (Fig. 8(c)), these differences are due to the effect of the depolarization field produced by $\vec{P}$.

5.2.2. Temperature dependence of soft mode in STO18

Figure 13 is the temperature dependence of Raman spectra for different $\vec{K}_p$ directions.

In Fig. 13(a) only the broad and underdamped mode $TO(A_1)$ softens and becomes weaker on approaching T_c as it should be. In contrast, Fig. 13(b) shows that two modes, $TO(A_1)$ and

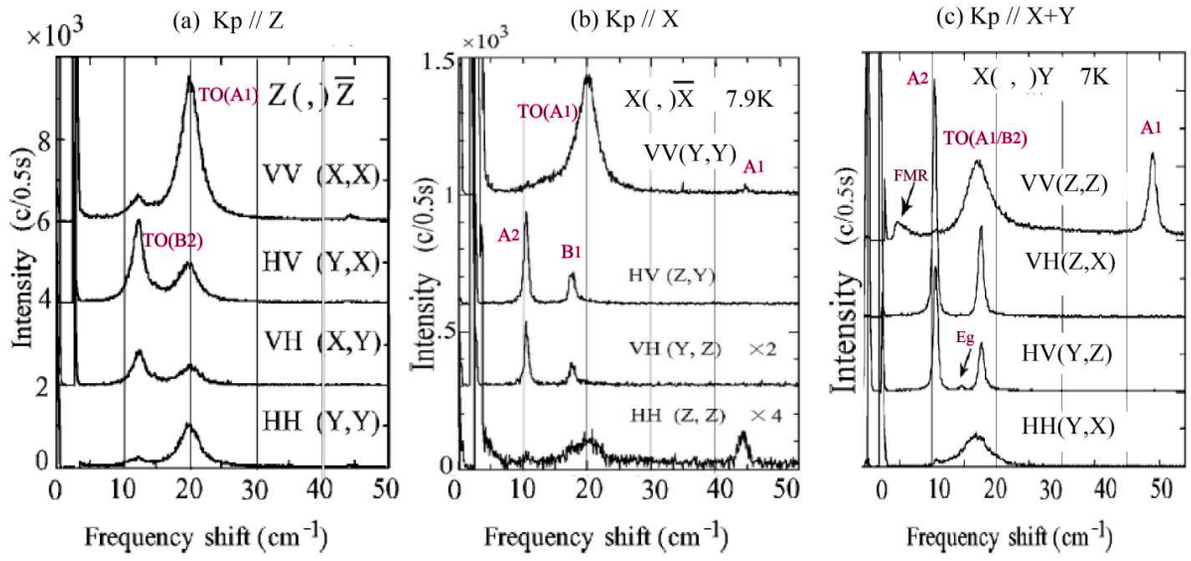

Figure 11. Polarized spectra at the lowest temperature for different propagation vector $\vec{K}_p$. (a) $\vec{K}_p$ // Z, (b) $\vec{K}_p$ // X, and (c) $\vec{K}_p$ // X + Y. Assignment of the peaks are given in red letters. Arrows in (c) are the spurious modes due to the paraelectric structure existing below T_c as the matrix of ferroelectric domains.

$TO(B_2)$ clearly soften. It is clear that frequencies of the soft modes never go down to zero. Instead in the $\vec{K}_p$ // Z spectra, in addition to the soft modes, a quasi-elastic mode appears near T_c (arrows in Fig. 13(b)). It is observed not only below T_c but also above T_c. Moreover, it is observed only when $\vec{K}_p$ is out of the X-Y plane such as for $\vec{K}_p$ // Z and $\vec{K}_p$ // Z + Y [36, 37].

The absence of the quasi-elastic mode in $\vec{K}_p$ // X (Fig. 13(b)) implies that it is *not* an overdamped soft mode as in the KDP case (section 4.1) but is a relaxational mode originated from the large fluctuations of $\vec{P}$ near T_c in the X-Y plane.

Another peculiar nature of the ferroelecticity of STO18 is the fact that even for a sample with 99% substitution, STO18 is *not* homogeneous contrary to the report by Taniguchi et al. [39], because the ferroelectric domains with $\vec{P}//X$ and $\vec{P}//Y$ coexist in the matrix of the paraelectric structure. The appearance of the spurious peaks in the $\vec{K}_p$ // X + Y spectra (Fig. 13(c)), which is FMR (Ferroelectric Micro-Domain) intrinsic to STO16, verifies the inhomogeneity of STO18.

The presence of the quasi-elastic mode in $\vec{K}_p$ // Z and its absence in $\vec{K}_p$ // X in STO18 were also reported by the independent two reports by Takesada et al. [17, 38] and Taniguchi et al. [39], respectively. As mentioned above, however, their conclusions are inconsistent with our results. Therefore, let us discuss briefly their results from our point of view.

a. Perfect softening of the Slater mode in STO18 was claimed in ref. [17] using a high-resolution spectrometer. Their results, however, are based on *only* the spectra with $\vec{K}_p$ // Z. Above T_c, they assign a *very weak bump* below 5 cm^{-1} sitting on the strong quasi-elastic (our relaxational) mode as the underdamped soft mode $TO(E_u)$. But below T_c, no such a narrow mode is observed and the strong quasi-elastic (our relaxational) mode is

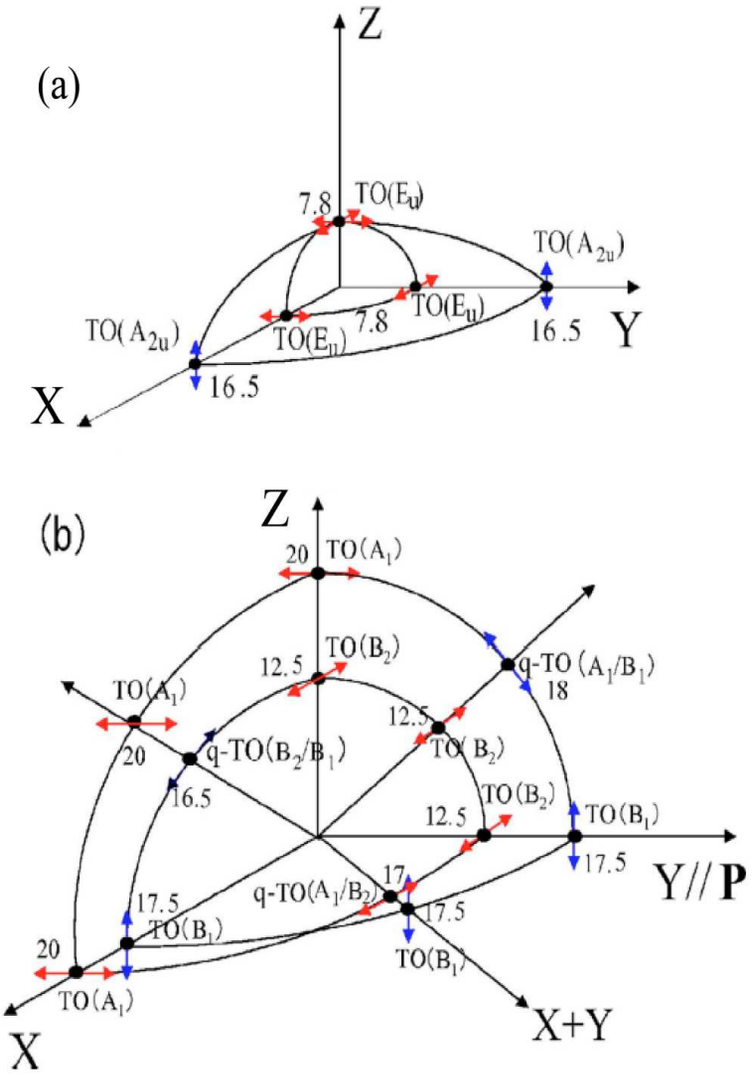

Figure 12. Ferroelectric soft-mode frequency surfaces for various directions of phonon propagation vector $\vec{K}_p$. $X = [110]_c$ and $Y = [1\bar{1}0]_c$ are the crystal axes of the tetragonal structure. (a) In the paraelectric phase near T_c. (b) In the ferroelectric phase well below T_c. Figure 12(b) is drawn for the case of $\vec{P} \,//\, Y$. Since in a sample of STO18, domains with $\vec{P} \,//\, X$ and $\vec{P} \,//\, Y$ coexist (in the matrix of paraelectric phase), observed spectra are the sum of the similar figure with the X and Y axes exchanged. Red arrows are the displacements in the X-Y plane and blue arrows are those out of the X-Y plane.

suddenly assigned as the overdamped soft modes $TO(A_1)$ and $TO(B_2)$. (We note that the lowest mode is *not* A_1 *but* B_2 contrary to the assignment by Takesada et al. [17].) From the computer fitting of the overdamped spectra below T_c, they obtain the extremely steep dropping of the frequency of $TO(B_2)$ down to zero. However, as mentioned in the case of KDP, such analysis is very ambiguous and the sudden qualitative change of the soft mode at T_c is unnatural. From these results they concluded that STO18 is an ideal displacive-type ferroelectrics induced by the Slater-type soft mode. If such a perfect softening took place at T_c it would be much more clearly observed in the $\vec{K}_p \,//\, X$ spectra, since as shown

http://dx.doi.org/10.5772/60613

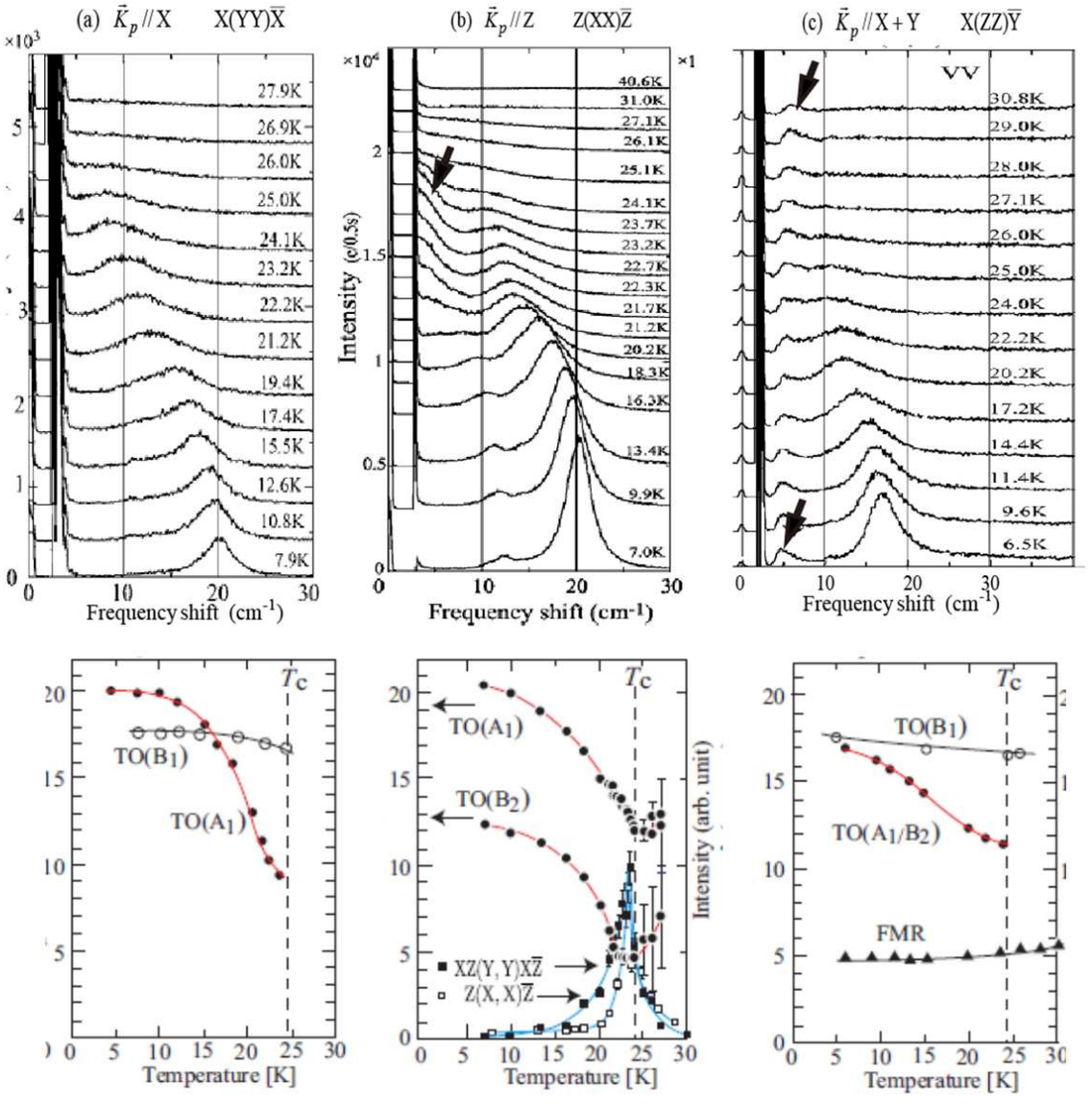

Figure 13. Temperature dependence of Raman spectra for different propagation directions: (a) $\vec{K}_p$ // X, (b) $\vec{K}_p$ //Z, (c) $\vec{K}_p$ // X + Y. The spectra for $\vec{K}_p$ // Y was identical to those for $\vec{K}_p$ // X. Note that in (b), a relaxational mode (blue lines) appears near T_c and in (c), a spurious mode (the arrows) is seen at about 5 cm^{-1} and no *pure* TO(A$_1$) is observed.

in Fig. 13(a), in the $\vec{K}_p$ // X spectra no quasi-elastic mode appears near T_c. Furthermore, if the perfect softening were related to the Slater-type mode, the direction of $\vec{P}$ should be parallel to cubic axis, which contradicts our results. Therefore, the essential difference between their interpretation and ours cannot be attributed to the difference of the resolution of the spectra.

b. Another essentially incorrect result was reported by Taniguchi et al. related to the homogeneity of STO18 [39]. They measured O^{18} concentration dependence of Raman spectra for $SrTi(O^{18}_x\ O^{16}_{1-x})_3$. In this paper, they measured the spectra again *only* with a

single $\vec{K}_p$, not $\vec{K}_p$ // Z but $\vec{K}_p$ // X, in which the quasi-elastic mode is absent. Then it was concluded that the homogeneous ferroelectric phase changes into theferroelectric-paraelectric phase coexistence state as thesystem approaches quantum critical point $x = 0.33$ and that highly substituted STO18 undergoes the ideal soft-mode-type quantum phase transition. As the evidence of the criticality, they claim that the mode at 15 cm^{-1} which is the E_g mode intrinsic to the paraelectric phase appears only in the low substitution samples below $x = 0.33$. However, as we have shown in the $\vec{K}_p$ // X + Y spectra (Fig. 13(c)), in addition to the FMR at 5 cm^{-1}, the E_g mode at 15 cm^{-1} (in our case 14.5 cm^{-1}) is certainly observed even in a very highly substituted sample with $x = 0.99$. This is a clear evidence of the existence of the paraelectric phase as the matrix of the ferroelectric domains. In other words, the *inhomogeneity is the intrinsic property* of STO18. Therefore, the transition of STO18 with high x is *not* the ideal (homogeneous) soft-mode-type quantum phase transition. In this case, they should have measured the $\vec{K}_p$ dependence more carefully, especially the $\vec{K}_p$ // X + Y spectra, since they have noticed from our results [36] that $\vec{P}$ is not along the cubic axes which suggests that the soft mode cannot be the Slater mode.

5.2.3. Why the soft mode is not the slater mode ?

The reason why $\vec{P}$ is not along the cubic axes (as expected from the softening of the Slater mode) but along the tetragonal axes would be closely related to the existence of the rhombohedral (parallel to $[111]_c$) nano-scale clusters in STO18 ,which were found in the NMR experiment by Blinc et al. [40]. They revealed that below 70 K rhombohedral polar clusters are formed in the tetragonal matrix. These clusters subsequently grow in concentration, freeze out, and percolate, leading to an inhomogeneous ferroelectric state below T_c. This shows that the elusive ferroelectric transition in STO-18 is indeed connected with local symmetry lowering and implies the existence of an order–disorder component in addition to the displacive soft mode one.

Referring to this result we have shown in a recent paper [37] that the dipole interaction between the rhombohedral polar clusters is the very probable reason for the formation of $\vec{P}//[110]_c$. The calculation shows that a pair of dipoles located in the same X-Y plane gives the strongest attractive interaction than any other possible pair interaction. The unification of such a pair of rhombohedral polar clusters generates $\vec{P}$ parallel *not* to the cubic axes but to the tetragonal axes. Spontaneous polarization $\vec{P}$ generated by this process would percolate and grow to the macroscopic ferroelectric domains.

Thus, the dipole interaction model is consistent with various peculiarities observed in the Raman spectra [36], such as the inhomogeneity, the imperfect softening, and the appearance of the relaxational mode near T_c. The origin of the relaxational mode observed near T_c would be the increase of the orientational fluctuations of $\vec{P}$ in the X-Y plane. Its coupling with the soft mode propagating along the Z axis would suppress the perfect softening.

Finally, we admit that the question "why the isotope substitution of O^{16} by O^{18} makes the ferroelectric transition possible in $SrTiO_3$" has not yet been fully solved.

6. LO/TO splitting in the ferroelectric Ice-XI

6.1. Structure of Ice-XI

The most common solid phase of water at normal pressure is the hexagonal ice (ice-Ih, D_{6h}^4, $P6_3/mmc$) which freezes at 273 K. In the Ih phase, however, due to the so-called ice-rules (Bernal–Fowler rules), protons on the hydrogen bonds are randomly distributed and below 100 K protons essentially freeze in place, leaving them disordered [41]. The residual entropy $S_{res} = R\ln(2/3)N$ [42] predicts the existence of the proton ordered state phase (known as ice-XI), but it would take a geological scale of time to transform into the ordered phase. In 1972, Kawada succeeded in obtaining the ice XI crystal at normal pressure by doping a small amount of KOH [43]. The calorimetric study [44] confirmed that ice-XI is stable for H_2O below $T_c = 72$ K. As shown in Fig. 14, in both ice-Ih and ice-XI, four water molecules are in a unit cell. In ice-XI, the c-component of the dipole moment of each H_2O molecule aligns ferroelectrically and the b-component aligns anti-ferroelectrically.

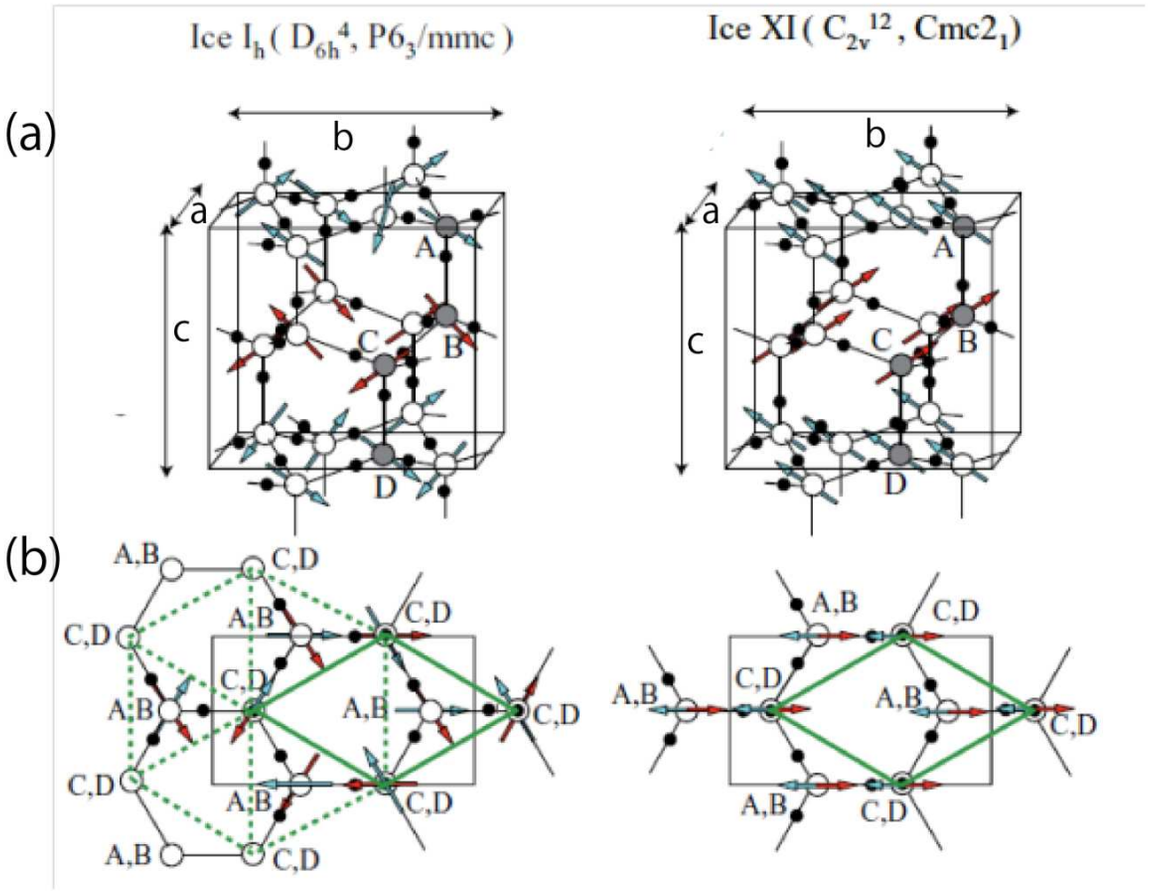

Figure 14. (a) Structures of ice-Ih and ice-XI. Four water molecules A, B, C, and D are in a unit cell [45]. (b) Projection to a–b plane. A unit cell is shown by the rhombus (thick green). The dotted hexagon shows the ice-Ih structure. Arrows represent the dipole moment of each molecule.

In contrast to neutron and theoretical studies, spectroscopic studies on ice-XI phase are very few. This is primarily because of the difficulty in growing a single crystal suitable for optical measurements. Recently, we have succeeded in growing a single crystal of ice-XI, which enabled us to measure the polarized Raman spectra [46]. Since the transition from Ih to XI is strongly of first order, no soft mode is expected for this transition. To observe whether the ferroelectric order was realized in our samples or not, the effect of the external electric field was tested on the sharp peak at 610 cm^{-1} which appears only in ice-XI. Although the effect was not significant compared to the ferroelectric soft mode in $SrTiO_3$ (Fig. 8(c)), the electric field (max 4 kV/cm) applied along the c-axis certainly increased its Raman intensity.

Figure 15(a) is the comparison of the wide frequency range spectra between ice-Ih and ice-XI measured with low resolution. Changes in the spectra were clearly recognized in the translational (below 350 cm^{-1}), librational (350–1200 cm^{-1}) and the stretching (above 2800 cm^{-1}) mode range. The polarization dependences of these spectra were analyzed satisfactorily. The bending mode range (1300–2700cm^{-1}) was too complicated to assign them properly [46].

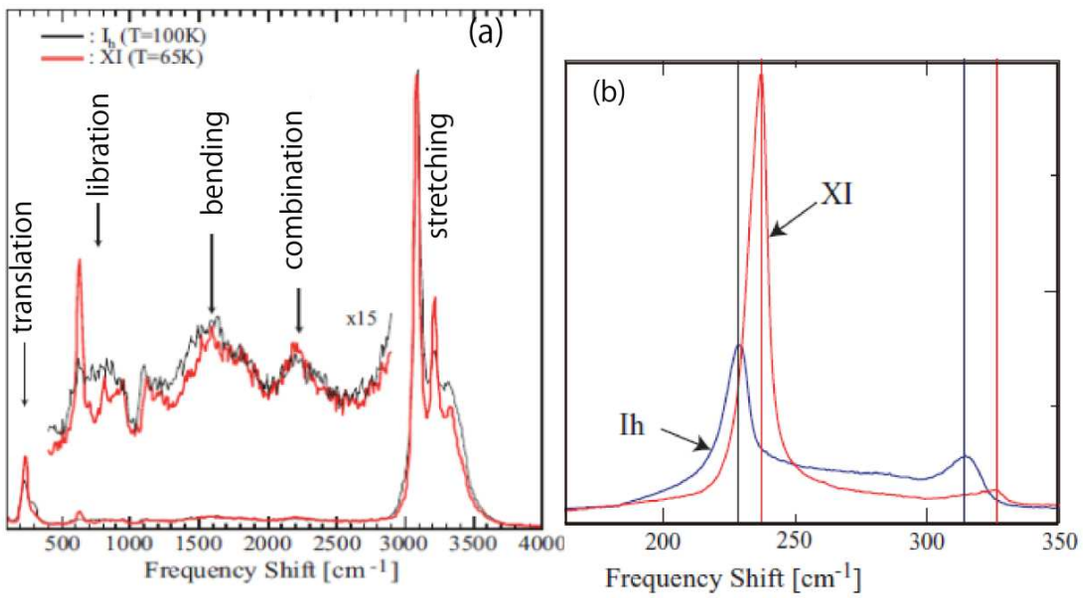

Figure 15. (a) Raman spectra in a wide frequency range. Scattering geometry is a(c, ∗)b with no polarization analyzer. Ice-XI is in red and ice-Ih (heated above T_c) is in black. (b) High-resolution Raman spectra in the translational mode range. Scattering geometry is a(cc)b Very strong peak at 237 cm^{-1} which corresponds to the A_1 component of LO is observed [46].

6.2. LO/TO splitting of the translational mode

LO/TO splitting of polar modes in ice-Ih has been a topic of long-standing discussion and particularly the translational mode spectra below 350 cm^{-1} were the controversial subjects. In 1991, Klug et al. [47] suggested from the analysis of IR reflection spectra of ice-Ih that a peak near 230 cm^{-1} is TO mode and the corresponding LO mode would be about 4 cm^{-1} higher than the TO. However, no direct evidence of the LO/TO splitting has yet been provided. Therefore,

measurement of the Raman spectra of ice-XI and comparison with that of ice-Ih are important to solve the long-standing questions.

In the higher-resolution spectra in ice-XI, clear polarization dependences were observed and successfully assigned most of the translational modes by taking into account the depolarization effect based on the simplified point mass model for each water molecule [46].

Displacements of the water molecules of the related translational modes are shown in Fig. 16. Among the 9 translational modes in ice-Ih, the degenerate E_{1g} and E_{2g} are lifted as $E_{2g} \rightarrow A_1 + A_2$ and $E_{1g} \rightarrow B_1 + B_2$, respectively. Although the displacement patterns are similar for these modes, the frequencies of the modes parallel to $\pm b$ axes are expected to become higher than those parallel to the a axes due to the depolarization field. Therefore, for the case of $\vec{K}_p // c$, LO/TO splitting is expected for the modes shown in the squares in Fig. 16.

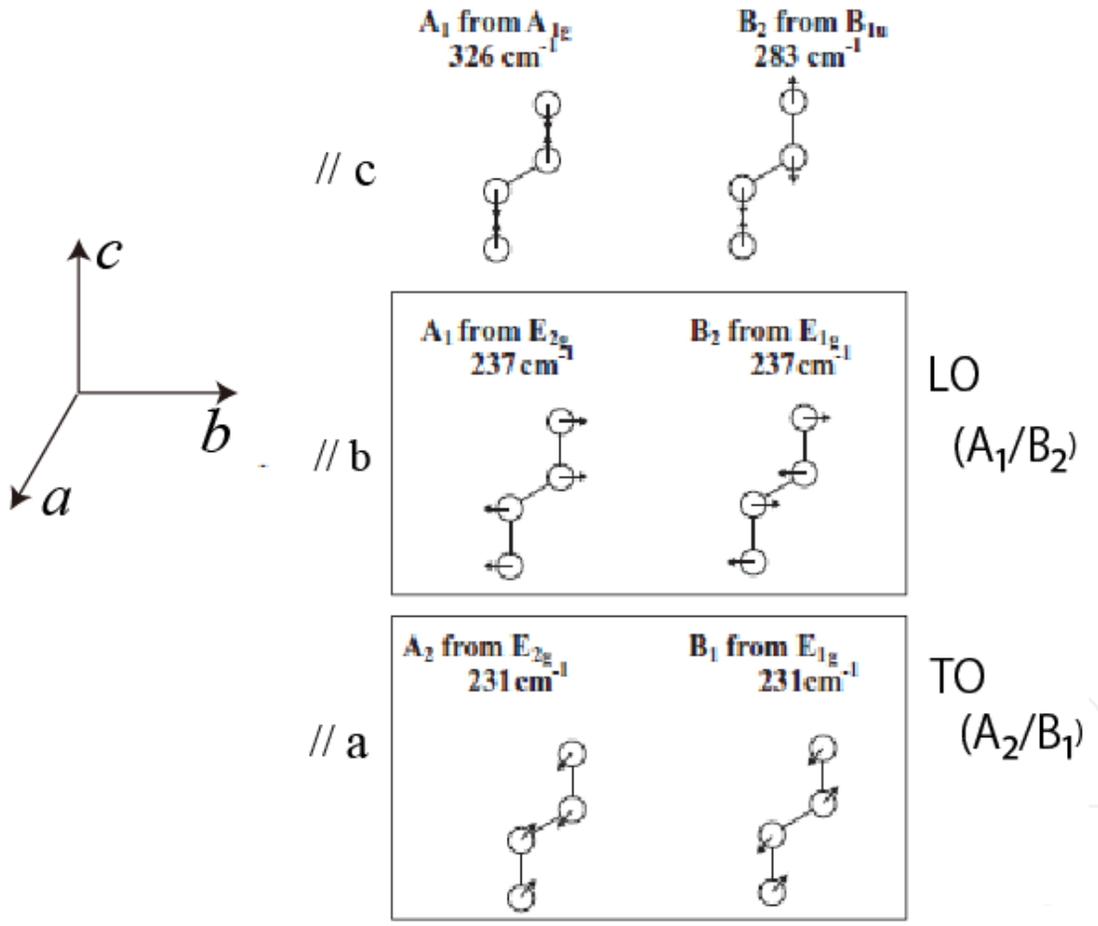

Figure 16. Dsplacement patterns and the symmetry of translational modes of ice-XI. The modes parallel to $\pm b$ axes are LO (237 cm^{-1}) and those parallel to a axes are TO mode (231 cm^{-1}).

The assignment of LO/TO splitting was confirmed by the $\vec{K}_p$ dependence of Raman spectra shown in Fig. 17. The most important feature is the fact that the very strong mode at 237 cm^{-1} is seen only in the geometry b(c, c)$\bar{b}$ (Fig. 17(a)) and in a(c, c)b in Fig. 15(b). In all other

geometries and polarizations, no frequency shift is observed. This means that the shift of the peak from 231 cm^{-1} to 237 cm^{-1} takes place only when $\vec{K}_p$ has a component parallel to the *b*-axis. In other words, the modes at 237 cm^{-1} should be assigned as the LO modes while the mode at 231 cm^{-1}, of which displacements are perpendicular to *b* is the corresponding TO mode. When the effect of the local depolarization electric field is larger than the crystal anisotropy, the LO/TO character dominates the symmetry of modes. Therefore, it is more appropriate to assign the peak at 237 cm^{-1} as the LO mode with mixed symmetry of A_1/B_2 and the peak at 231 cm^{-1} as the TO mode with mixed symmetry of A_2/B_1. Contribution of B_2 component to LO was confirmed in the a(b,c)c spectra shown in Fig.7 of ref.[46].

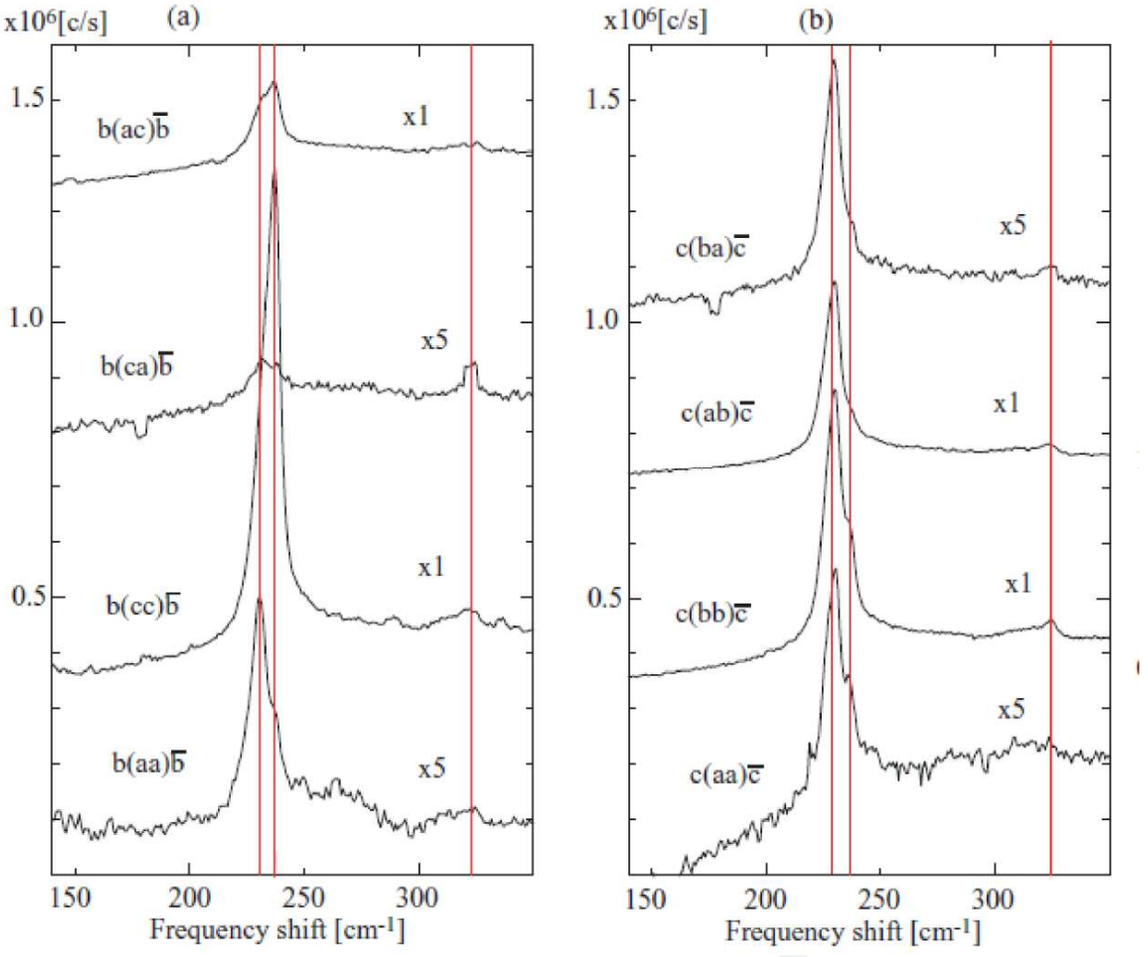

Figure 17. Dependence of the Raman spectra on the phonon propagation direction $\vec{K}_p$. (a) $\vec{K}_p // b$ and (b) $\vec{K}_p // c$. Very strong peak at 237 cm^{-1} is observed only in (cc) spectrum in (a) corresponding to the A_1 component of LO.

The present result is the first experimental confirmation of the LO/TO splitting in ice. The 6±0.5 cm^{-1} of the LO/TO splitting agrees with 4cm^{-1} obtained in the IR reflection spectra of ice-Ih by Klug et al. [47] and also close to 10 cm^{-1} of the calculation by Marchi et al. [48]. Another feature of the LO (A_1/B_2) mode at 237 cm^{-1} is the fact that its intensity is strong only in the spectra with polarization (cc). From the selection rule, the A_1 mode is active

also in (aa) and (bb). However, the intensity in (aa) and (bb) is much weaker than that in (cc). This indicates that the Raman polarizability tensor $R_{cc} = \partial\alpha_{cc}/\partial Q_{A1}$ is much larger than R_{bb} or R_{aa}. Large R_{cc} may be attributed to the depolarization field parallel to the c-axis caused by the partial ferroelectric order in ice-XI.

The behavior of the highest translational mode near 326 cm^{-1} seems to be more complicated. It does not depend on $\vec{K}_p$ and polarization. Its intensity does not significantly increase by the transformation from ice-Ih to ice-XI. The differences from other translational modes cannot be explained by the simple point mass model. Maybe the modes with the displacement parallel to the c-axis (upper two modes in Fig. 16), are more complicated due to the long-range Coulomb force along the c-axis, which induces the interaction with other degrees of freedom such as the librational motion of water molecules.

6.3. Raman spectra of stretching modes in Ice-XI

Interpretation of Raman and infrared spectra of ice in the OH stretch region above 2800 cm^{-1} has been also a topic of long-standing discussion. The lowest Raman peak and the central IR peak were assigned to in-phase symmetric (ν_1) and antisymmetric stretch (ν_3) vibrations of the two O-H bonds in a single water molecule, respectively (See Fig.18(c)). Whalley summarized the spectral features in ice-Ih and assigned the four stretching bands in terms of LO/TO splitting of ν_3 vibrations as follows [49]:

band 1 3083 cm^{-1} = ν_1 (in-phase)

band 2 3209 cm^{-1} = ν_3 (TO)

band 3 3323 cm^{-1} = ν_3 (LO)

band 4 3420 cm^{-1} = ν_1 (out-of-phase)

Figure 18 shows the polarized Raman spectra in the range 2900–3600 cm^{-1} of single crystal of ice-Ih and ice-XI at about 60 K. Spectra are composed of four bands and look similar for both phases except for the significant intensity increase in the depolarized spectra of the band 1 such as a(b, c)b [50].

In order to see whether Whalley's assignments are valid in ice-XI or not, spectra for different propagation vectors $\vec{K}_p$ were measured. Observed spectra for $\vec{K}_p // c$ and //b are, however, almost identical to the spectra for $\vec{K}_p \perp c$ shown in Fig. 18(b). The frequency of the band 3 (3327 cm^{-1}) does not vary in c(,)$\bar{c}$ or in b(,)$\bar{b}$. Furthermore, as shown in Fig.13 of ref. [50], the polarized Raman spectra (aa) and (bb) have the same intensity as that of (cc). This means that, in contrast to the translational mode case, Raman intensity of the stretching modes is not affected by the long-range electric field produced by the transformation to ice-XI. Thus, from the present work we could not find any direct evidence of band 3 being the ν_3 (LO) mode. We assign the band 2 and 3 simply as the in-phase and out-of-phase of ν_3 mode. Although the lowest frequency band 1 is no doubt the in-phase symmetric stretching mode ν_1, the origin of the highest frequency weak band ν_4 near 3400 cm^{-1} is still not certain. Present results show that for the

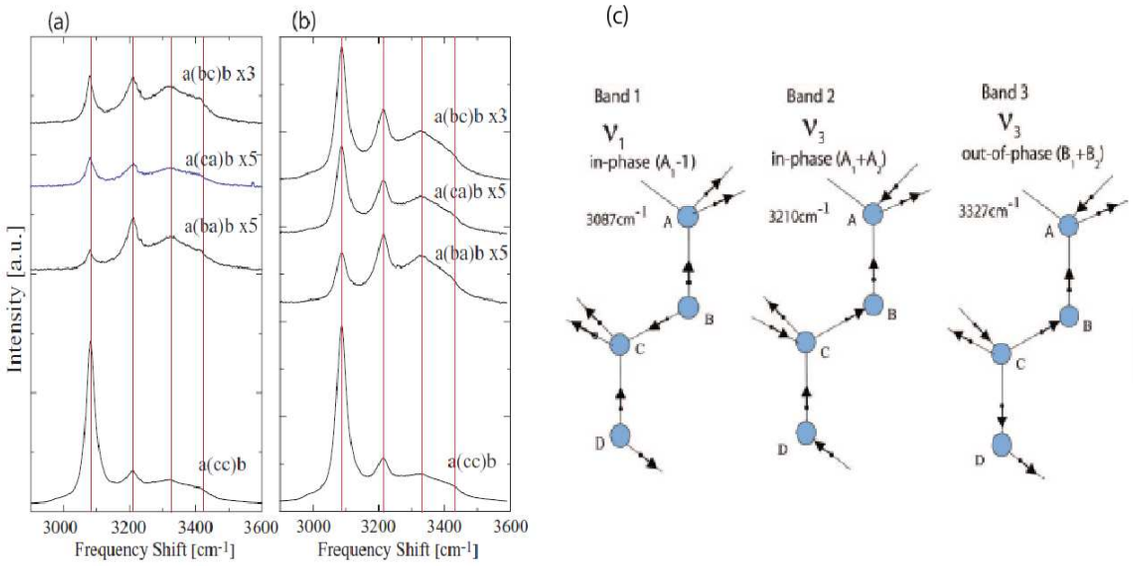

Figure 18. Polarization dependence of Raman spectra at about 60 K in the stretching mode range. (a) Ice-Ih and (b) ice-XI. Scattering geometries are a(,)b. (c) Displacement pattern of stretching mode corresponding to band 1,2 and 3. Only the depolarized spectra of band 1 significantly increase in ice-XI.

stretching vibrations in ice I (Ih and XI), the effect of the short-range intermolecular coupling is dominant than the long-range interaction produced by the proton ordering [50].

7. Summary and conclusions

Lattice vibrations that carry an electric dipole moment (polar phonons) have radically different long-wavelength properties from nonpolar vibrations. Soft modes in ferroelectric crystals are the typical polar modes. In this chapter, characteristics of soft modes and Raman spectra of polar modes were described mainly based on our experimental results.

In section 2, general properties of polar modes are given. In section 3, the physical meaning of the susceptibility $\chi_Q(\omega)$ such as the damped-harmonic-oscillator (DHO) and the Debye-type relaxation, which are often used in the analysis of the overdamped soft mode Raman spectra, was discussed in terms of the proposed generalized form of susceptibility (GVWF).

In section 4, the difficulty in discriminating between the displacive-type and the order–disorder-type phase transition is shown in the case of KDP. Particularly, the analysis of the overdamped soft mode spectra using an arbitrary susceptibility could be very ambiguous.

In section 5, the peculiar nature of the Raman spectra related to the ferroelectric transition of the isotope exchanged ferroelectric $SrTiO_3$ (STO18) was discussed. From the spectra with various propagation directions ($\overline{K}_p$), it was shown that the spontaneous polarization $\vec{P}$ is not a result of the freezing of the Slater mode. Therefore, the ferroelectric phase transition of STO18 is *not* an ideal soft mode type quantum phase transition.

In section 6, the first clear evidence of the LO/TO splitting in the Raman spectra of the translational mode in the proton-ordered (ferroelectric) ice-XI was given.

To conclude, the following points must be taken into account for the correct interpretation of Raman spectra in ferroelectric crystals:

1. The analysis of the overdamped mode by the computer fitting depends on the model and the used susceptibility function. The results would be often ambiguous as in the cases of KDP.
2. The effect of the depolarization field caused by the spontaneous polarization $\vec{P}$ below T_c must be taken into account by the measurement of the propagation direction ($\overline{K}_p$) dependence, as in the cases of STO18 and ice-XI.
3. The influence of domains and the possible inhomogeneity in the sample must be taken into account. as in the cases of KDP and STO18.
4. The selection rules and the displacement patterns must be taken into account by the polarized Raman spectra using different scattering geometries, as in the case of STO18 and ice-XI.
5. The evidence of the LO/TO splitting should be obtained by the measurement of the propagation direction ($\overline{K}_p$) dependence, as shown in ice- XI.

Acknowledgements

The author thanks Yasunari Takagi for the collaboration during the analysis of the Raman spectra of KDP and the generalization of the susceptibility. He also thanks Kohji Abe for his long-term collaboration and valuable discussions during the studies on STO18 and ice-XI. We wish to thank Prof. Mitsuru Ito of Tokyo Institute of Technology for providing the high-quality sample of STO18. The experiments were supported by the enthusiastic collaboration of a number of graduate students in UEC.

Author details

Takeshi Shigenari*

Address all correspondence to: shigenar@pc.uec.ac.jp

Department of Applied Physics and Chemistry, The University of Electro-Communications, Chofu-shi, Tokyo, Japan

References

[1] P.W.Anderson, Fizika dielektrikov (Akad. Nauk SSSR) 290 (1960) ; W.Cochran, Adv. in Phys. 9 387 (1960).

[2] J.M.Worlock, *Structural phase transitions and soft modes* (Universitetforlaget, Oslo). 329 (1971).

[3] J.F.Scott, Rev.Mod.Phys. 46 83 (1974).

[4] W.Hayes and R.Loudon, *Scattering of Light by Crystals*, Dover Publications, Inc. Mineola, New York 1978.

[5] C.H.Henry and J.J.Hopfeld, Phys.Rev.Lett. 15 964 (1965).

[6] Exception of the Worlock's conjecture is given by T.Shigenari, Phys.Lett. 46A 243 (1973).

[7] Y.Takagi and T.Shigenari, J.Phys.Soc.Jpn. 39 440 (1975).

[8] J.H.Van Vleck and V.F.Weisskopf, Rev.Mod.Phys. 17 227 (1945).

[9] Y.Takagi and T.Shigenari, J.Raman Spectroscopy 10 158 (1981) ; Y.Takagi, J.Phys.Soc.Jpn. 47 567 (1979).

[10] I.P.Kaminov and T.C.Damen, Phys.Rev.Lett. 20 1105 (1968).

[11] R.Blinc, J.Phys.Chem.Solids 13 204 (1960).

[12] W.Cochran, Phil.Mag. Suppl. 10 401 (1961).

[13] P.G.de Gennes, Solid St.Comm. 1 132 (1963).

[14] M.Tokunaga, Prog.Theor. Phys. (Kyoto) 36 357 (1966).

[15] Y.Takagi and T.Shigenari, J.Phys.Soc.Jpn. 47 576 (1979).

[16] Y.Tominaga and H.Urabe, Solid St.Comm. 41 561 (1982).

[17] M.Takesada, M.Itoh and T.Yagi, Phys.Rev.Lett. 96 227602 (2006).

[18] Y.Takagi, J.Phys.Soc.Jpn. 47 567 (1979).

[19] T.Shigenari and Y.Takagi, J.Phys.Soc.Jpn. 31 312 (1971). Temperatures were corrected in T.Shigenari, Butsuri 30 733 (1975). (in Japanese)

[20] Y.Tominaga, H.Urabe and M.Tokunaga, Solid State Comm. 48 265 (1983) ; Y.Tominaga and M.Tokunaga, KotaiButsuri(Solid state physics) 18 724 (1983). (in Japanese)

[21] T.Shigenari, Kotai Butsuri (Solid state physics) 23 600 (1988). (in Japanese)

[22] K.K.Kobayashi, J.Phys.Soc.Jpn. 24 497 (1968).

[23] T.Shigenari and Y.Takagi, Solid State Comm. 11 481 (1972) ; Y.Takagi and T.Shigenari, J.Opt.Soc.America 63 995 (1973).

[24] K.A.Müller and H.Burkard, Phys. Rev. B 19 3593 (1979): R.A.Cowley, Phys.Rev. 134 A981(1964).

[25] M.Itoh, R.Wang, Y.Inaguma, T.Yamaguchi, Y.-J.Shan and T.Nakamura, Phys. Rev. Lett. 82 3540 (1999).

[26] R.A.Cowley, Phys. Rev. 134, A981 (1964).

[27] A.Yamanaka, M.Kataoka, Y.Inaba, K.Inoue, B.Hehlen and E.Courtens, Europhys. Lett. 50 688 (2000).

[28] A.S.Barker, Jr. and R.Loudon, Rev.Mod. Phys. 44 18 (1972).

[29] G.Shirane and Y.Yamada, Phys. Rev. 177 858 (1969).

[30] K.Inoue, Ferroelectrics 52 253 (1983) ; H.Vogt, Phys. Rev. B51 8046 (1995).

[31] P.A.Fleury and J.M.Worlock, Phys. Rev. Lett. 18 655 (1968) ; P.A.Fleury and J.M.Worlock, Phys. Rev. 174 613 (1968).

[32] T.Shigenari and H.Ebashi, J.Phys.C: Solid State Phys. 14 969 (1981).

[33] T.Shigenari, Phys.Lett. 98A 63 (1983).

[34] Y.Noda, Private Communications. (2010).

[35] Y.Tsujimi, M.Kobayashi, Y.Minaki, M.Nakanishi, R.Wang, M.Itoh and T.Yagi, Ferroelectrics 304 71 (2004).

[36] T.Shigenari, K.Abe, T.Takemoto, O.Sanaka, T.Akaike, Y.Sakai, R.Wang and M.Itoh, Phys. Rev. B74 174121 (2006).

[37] T.Shigenari, T.Nakano and K.Abe, Europhys.Lett. 94 57001 (2011).

[38] M.Takesada, M.Itoh and T.Yagi, Phys.Rev.Lett. 96 227602 (2006) ; M.Takesada, M.Itoh, A.Onodera and T.Yagi, Ferroelectrics. 346 20 (2007).

[39] H.Taniguchi, M.Itoh and T. Yagi, Phys.Rev.Lett. 99 017602 (2007).

[40] R.Blinc, B.Zalar, V.V.Laguta and M.Itoh, Phys.Rev.Lett. 94 147601 (2005).

[41] J.D.Bernal and R.H.Fowler, J. Chem. Phys. 1 515 (1933).

[42] L.Pauling, J. Am. Chem. Soc. 57 2680 (1935).

[43] S.Kawada, J. Phys. Soc. Jpn. 32 1442 (1972).

[44] T.Matsuo, Y.Tajima and H.Suga, J. Phys. Chem. Solids. 47 165 (1986).

[45] R.Howe and R.W. Whitworth, J. Chem. Phys. 90 4450 (1989).

[46] K.Abe and T.Shigenari, J. Chem. Phys. 134 104506 (2011).

[47] D.D.Klug, J.S.Tse and E.Whalley, J. Chem. Phys. 95 7011 (1991).

[48] M.Marchi, J.S.Tse and M.L.Klein, J. Chem. Phys. 85 2414 (1986).

[49] E.Whalley, Can. J. Chem. 55 3429 (1977).

[50] T.Shigenari and K.Abe, J. Chem. Phys. 136 174504 (2012).

IntechOpen